सत्यमेव जयते

BRIT Bulletin 2022

Scientific Magazine

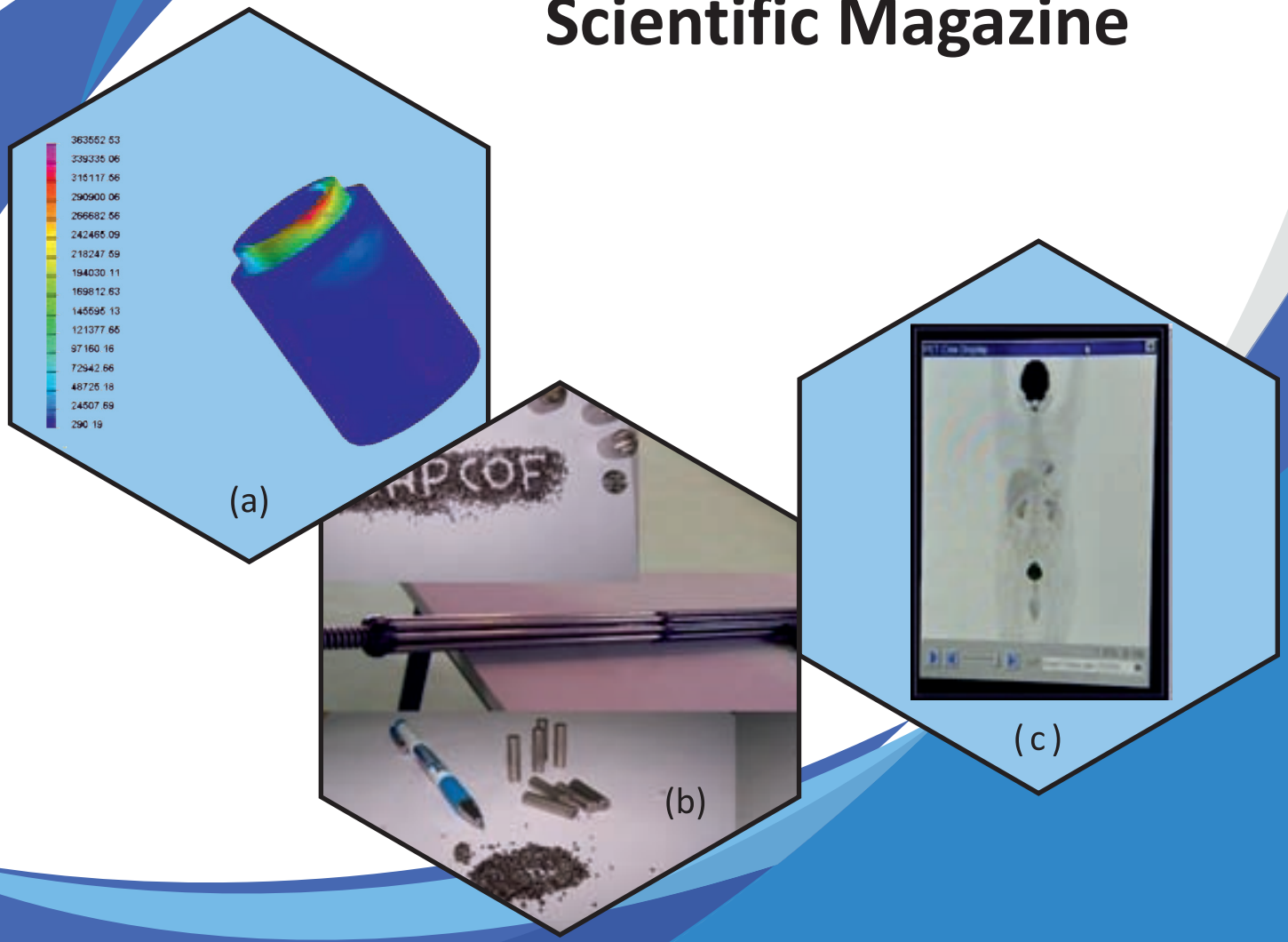

GOVERNMENT OF INDIA
DEPARTMENT OF ATOMIC ENERGY
BOARD OF RADIATION & ISOTOPE TECHNOLOGY

BRIT Bulletin 2022

'Scientific Magazine'

Board of Radiation & Isotope Technology, DAE

TECHNOLOGIES FOR
NEW INDIA@75
आज़ादी का अमृत महोत्सव

सत्यमेव जयते

GOVERNMENT OF INDIA

DAE
Department of Atomic Energy

Front Cover: (a) Stress intensity on the tungsten component under 9m horizontal drop of the newly designed MTP 1200 transportation cask, which would be used to transport 1200 Ci of ^{99}Mo;
(b) Pellets, Slugs, Sub-Assemblies that constitute ^{59}Co Absorber rods, used in Nuclear Reactor;
(c) PET-CT Whole Body Scan of ^{18}F-FDG

Back Cover: Logo's for 75 Years of Independence celebrated as "Azadi Ka Amrit Mahotsav (AKAM)" during August 2021- August 2022.

Foreword

It gives me immense pleasure and pride to release the Publication of BRIT Bulletin-2022, which houses, brief communications, original research articles and review articles.

BRIT products utilize diversity of radioisotopes and devices using radiation technology for variety of users and these products are used for different applications. They are produced by skilled expertise to yield quality products, conforming to national and international standards. This is the reason behind BRIT's wide customer base, not only in India, but also abroad. The dedicated services towards societal benefits brought several accolades for BRIT in the last few years.

While serving the society with the existing products & services, it is equally important to constantly expand the state-of-art solutions across all the fields, and through our coordinated & consorted efforts, it is envisaged that BRIT will further grow and evolve into a global player.

The dynamic progress consistently made by BRIT since past three decades, either, independently, or, with collaborations with research organizations like BARC, IGCAR, VECC or RRCAT, is worth its mention. I am happy to witness few of these being showcased through scientific bulletins, which are published annually.

I am delighted to present you all 'BRIT Bulletin 2022', the contents of which are from various fields of science and technology. They are mainly towards studies of the new procedures and products or the performance & status of these in the present scenario.

I extend my appreciation and congratulate the Scientists and Engineers for their valuable contributions for BRIT Bulletin 2022.

Pradip Mukherjee

CONTENTS

Development of Organic Soluble ^{99}Mo-Based Novel Industrial Radiotracer for Identification of Leaky Components of Petroleum Refineries

Abhishek K. Sharma[1], Gaurav Agrahari[2]

[1]Radiopharmaceutical Laboratory (RPL), and [2]Industrial Application Services (IAS)

(Corresponding author: abhishek.sharma@britatom.gov.in)

Abstract

Molybdenum-99 (^{99}Mo) activity, in the form of ^{99}Mo-alfa-benzoin oxime (^{99}Mo-ABO) complex was developed as industrial radiotracer and its utility was tested in a diesel hydro-treater (DHDT) unit of a leading oil refinery. Aim of the study was to evaluate the suitability of the developed ^{99}Mo-ABO complex for radiotracer investigation at high temperature and high-pressure hydrocarbon stream. A methodology was developed to convert the aqueous solution of fission ^{99}Mo in to ^{99}Mo-ABO complex, suitable for mixing with organic phase. A radiotracer study was carried out to identify the leaky heat exchangers from a series of four heat exchangers using ^{99}Mo-ABO complex in organic phase as a novel industrial radiotracer. Reproducibility of the result was verified by using ^{99m}Tc in organic phase as another radiotracer. From the study it was found that the developed radiotracer'^{99}Mo-ABO complex' is suitable for industrial applications at high temperature and high-pressure hydrocarbon stream.

Introduction

Owing to stringent pollution control norms, there are strict quality control specifications on the concentration of sulfur in diesel produced in petroleum refineries. Therefore, in petroleum refineries diesel is hydro-treated to remove the sulphur to make it compliant with BS-VI Norms (sulphur < 10 ppm). Timely detection of any leak present in the stream of the hydro-treating unit is required for a good quality diesel product, a better production efficiency, occupational safety and to control environmental pollution[1][2][3]. Any deviation from the normal operating parameters such as product contamination, loss of pressure and loss of process efficiency indicates the presence of leak in the system[3][4].

In various petroleum refineries, diesel hydrotreater (DHDT) units are designed to treat the high sulphur distillates and cracked feed streams by employing a suitable catalyst and a hydrogen rich gas stream. This process removes the organic sulphur, oxygen and nitrogen compounds contained in the feed as well as it improves the cetane number of the desired diesel product. During this process, a large amount of heat is generated and recovery of the product heat is done by preheating the feed in a series of heat exchangers[2][3]. Most commonly used heat exchangers in the DHDT units of petroleum refineries are serially connected shell & tube type of breech-lock heat exchangers. Since the temperature and pressure involved are

very high, the various conventional techniques used for the identification of leaks in heat exchanger systems such as visual inspection, pressure change method, chemical reagent test, dye penetrant test, acoustic leak detection and mass spectrometry cannot be used on-line[4]. These conventional tests can be employed only for offline leak detection, which requires shutdown and hence, do not yield desired commercial benefits[1][3].

Generally, the diesel stream inside the breech lock heat exchangers during operation bears the pressure of 10-17.6 MPa and temperature of around 350-600°C. Sampling ports are not provided in this kind of heat exchanger system to avoid any fire hazards. Therefore, conventional tracers (non-radioactive tracers) cannot be used for leak detection during online operating conditions.

Application of radio-tracers offers online measurement due to penetrating nature of gamma rays which can be detected from outer surface of the heat exchanger system[1][5][6][7]. A common radiotracer for industrial application is ^{82}Br [$T_{1/2}$: 36 h; E : 1.32 MeV (26.8%), 0.55 MeV (70%)] in organic form[2][8][9]. However, high gamma energy of ^{82}Br may result in, cross peak detection at various other locations in surrounding heat exchangers thereby leading to misinterpretations. On the other hand, ease of availability, lower gamma energy and longer half-life of ^{99}Mo [$T_{1/2}$: 66 h; E : 740 KeV (12.8%), 181KeV (6.2%)] makes it a promising alternative to ^{82}Br.

A radiotracer study involves injection of a radiotracer of pre-calculated activity as sharp pulse using a specially designed injection system into the higher-pressure side of the heat exchanger system. Usually the pressure difference between shell side and tube side of the heat exchanger in DHDT unit is around 1.18-1.47 MPa. In case of any leakage in the heat exchanger, a fraction from the higher-pressure side of the injected radiotracer will flow to the lower pressure side[3][4]. The location and collimation of the radiation detectors are strategically chosen to avoid cross peak detection and to record statistically sufficient counts. The detectors are kept at the higher-pressure side inlet, higher pressure side outlet and lower pressure side outlets of the serially connected heat exchangers. Rise in the count-rate above background in the lower pressure side outlets of the heat exchangers indicates presence of the leakage.

The radiotracer study was carried out at DHDT unit of a petroleum refinery, identification of leaky heat exchangers was carried out using a newly developed industrial radiotracer ^{99}Mo-alfa-benzoinoxime (ABO) complex in the organic phase. Reproducibility of the result was verified by a proven industrial radiotracer, ^{99m}Tc [$T_{1/2}$: 6 h; E : 140 KeV] in organic phase[10][11][12][13].

Experimental

(a) Preparation of 99mTc radiotracer dissolved in organic phase

18.5 GBq of high specific activity ^{99}Mo, in the form of sodium molybdate (volume: 10 mL), was transferred into a lead shielded solvent extraction set-up (Fig.1), by applying vacuum. 20 ml of 5N NaOH solution was added to it. The solution was agitated by drawing air through the solution using a vacuum pump.

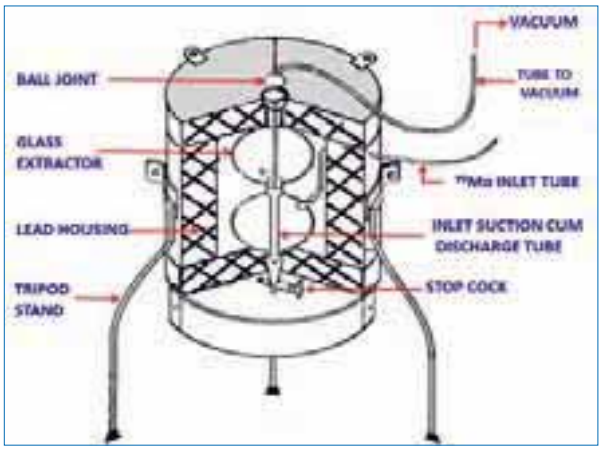

Fig.1: Lead shielded solvent extraction set-up

The solution contains ^{99}Mo, in transient radioactive equilibrium with its daughter isotope ^{99m}Tc. From this solution, ^{99m}Tc was recovered into the organic phase by solvent extraction using MEK. For extraction of ^{99m}Tc, 30 ml of MEK was added to the aqueous solution of sodium molybdate. The aqueous phase and the organic phase were equilibrated for 15-20 minutes by drawing air through the bottom of the extraction system using a vacuum pump. The mixture was allowed to settle for 5 minutes for phase separation. The aqueous layer forms the bottom layer, whereas organic layer (containing extracted ^{99m}Tc) forms the top layer. The organic layer (containing ^{99m}Tc) was separated and mixed with 500 mL of diesel for use in radiotracer investigation of heat exchangers system.

(b) Preparation of ^{99}Mo-ABO radiotracer dissolved in organic phase

The aqueous layer of the previous extraction, containing ^{99}Mo activity, was again taken into the solvent extraction set-up by a vacuum pump. To this solution, 10 mg of molybdenum carrier, in the form of sodium molybdate solution was added. The resultant solution was acidified by adding with concentrated HNO_3 to reach a final acidity of 3.5 M. The resulting solution was agitated for 30 minutes. Molybdenum in the aqueous solution was quantitatively precipitated with the drop wise addition of 21 mL of alfa-benzoin oxime (ABO) solution (2 mg L^{-1} in ethanol). The resulting mixture was then mixed with 30 mL chloroform and agitated by drawing air through the mixture. The ^{99}Mo-ABO precipitate got dissolved into the chloroform layer. The mixture was allowed to settle for 5 minutes. The chloroform layer which contains^{99}Mo activity in the form of Mo-ABO complex, forms the bottom layer. The bottom layer was collected and mixed with 500 mL of diesel for its use in leak detection study of heat exchangers system.

(c) Heat exchanger system

There are four heat exchangers in series viz. 09-EE-002A/B and 09-EE-003A/B as shown in Fig. 2. The reactor feed is introduced through the shell inlet of 09-EE-003A and travels sequentially through the shells of 09-EE-003B, 09-EE-002A and 09-EE-002B to the reactor. The final diesel product from the reactor flows counter current through the tubes in the order 09-EE-002B $\rightarrow$ 09-EE-002A $\rightarrow$ 09-EE-003B $\rightarrow$ 09-EE-003A. During its passage, heat is transferred from tube side diesel stream to shell side feed. The feed flowing in the shell side is at higher pressure than the diesel flowing in the tube side as seen from Table1. Since the sulphur content in the product diesel was higher than expected (>50 ppm), it was suspected that the feed is leaking in to the

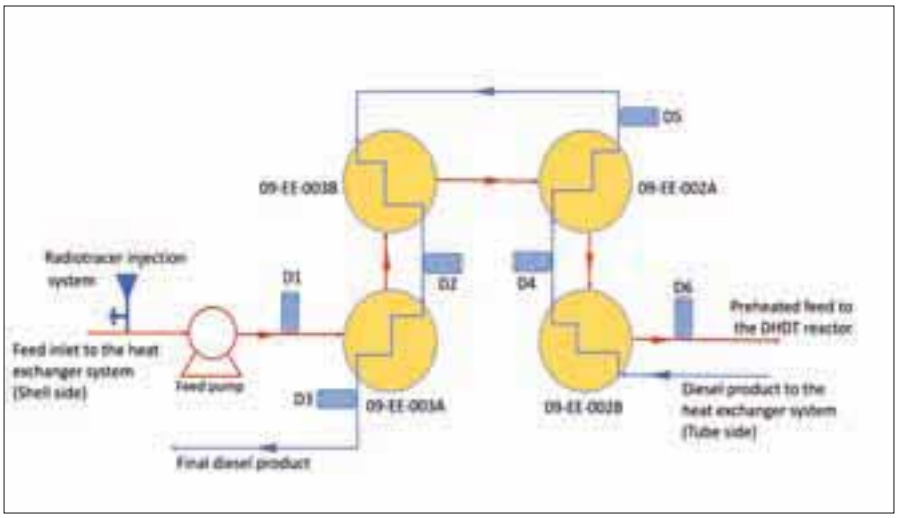

Fig. 2: Schematic of heat exchanger system showing injection system, feed pump and strategically located radiation detectors

Table 1 Characteristics of heat exchangers being studied

Tag No.		09-EE-002 A / B	09-EE-003 A / B
Description		Hot combined Feed Exchanger	Cold combined Feed Exchanger
Service	Shell	Hydrocarbons, H_2, H_2S	Hydrocarbons, H_2, H_2S
	Tube	Hydrocarbons, H_2, H_2S	Hydrocarbons, H_2, H_2S
Operating pressure (MPa)	Shell	11.96	12.06
	Tube	10.66	10.36
Operating temperature (°C)	Shell Inlet	195	80
	Shell Outlet	354	195
	Tube Inlet	408	234
	Tube Outlet	291	148

final diesel product. Hence, a radiotracer study was planned to identify the leaky heat exchanger.

(d) Radiotracer study

A first radiotracer injection was carried out using ^{99}Mo-ABO complex in organic medium. The pressure inside the feed inlet to the pump was 490-588 KPa. The radiotracer was injected as a sharp pulse using a specially fabricated injection system (Fig. 3) into the inlet of the feed pump. The radiotracer was first poured into the injection system and it was pushed to the main stream by pressurizing with nitrogen gas at about 980 KPa. The same procedure of injection and subsequent detection was repeated for the radiotracer ^{99m}Tc in organic phase.

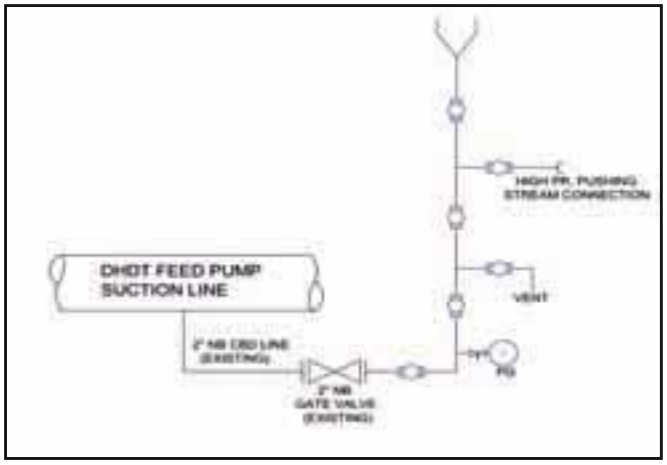

Fig.3: Schematic of the radiotracer injection system

The flow of radiotracer in the heat exchanger system, was monitored using NaI(Tl) scintillation detectors. The detectors were shielded using an approximately 5 cm thick lead collimator and jacketed for thermal insulation using Bakelite. Table 2 indicates the location of different detectors in the series of heat exchanger.

Table 2 Detector locations

Detector No.	Detector location
D1	Shell Inlet of 09-EE-003A
D2	Tube Outlet of 09-EE-003B
D3	Tube Outlet of 09-EE-003A
D4	Tube Outlet of 09-EE-002B
D5	Tube Outlet of 09-EE-002A
D6	Shell Outlet of 09-EE-002B

The count-rate data from each detector was acquired through a multi input data acquisition system (MIDAS). It offers collection and visualization of data in real time.

Results and Discussion

Solvent extraction method using MEK is well known process for separation of ^{99m}Tc activity from its parent isotope ^{99}Mo [14]. During the extraction process, ^{99m}Tc is recovered into the organic phase from alkaline aqueous layer (MEK). Organic phase, which contains recovered ^{99m}Tc, forms a homogenous solution with diesel which is suitable for radiotracer application [13]. Molybdenum in the aqueous layer was selectively precipitated with alfa-benzoin oxime (ABO) in acidic condition to separate ^{99}Mo from aqueous layer. Detailed investigation on the Mo-alfa-benzoin oxime precipitation process has been reported elsewhere [15].

In the present study, 3 M HNO_3 was added to the alkaline solution containing ^{99}Mo. The solution was left standing for 30 minutes to ensure the forming of the desired molybdenum species (MoO_2^{2+}) suitable for complexation with ABO. Addition of ABO (Mo: ABO weight ratio of 1:10) to the aqueous layer resulted in the formation of Mo-ABO complex, suitable for mixing with the organic phase.

Both the radiotracers were separately injected in to the system and their passage were monitored online through scintillation detectors. Radiotracer data was acquired for every 100 milliseconds. Data points for each detector were separately plotted to carefully analyze the results as shown in Fig. 4, Fig. 5, Fig. 6 and Fig. 7.

The first radiotracer study was carried out by injecting ^{99}Mo-ABO complex dissolved in diesel. The peak observed at a time of 15300 millisecond in the response

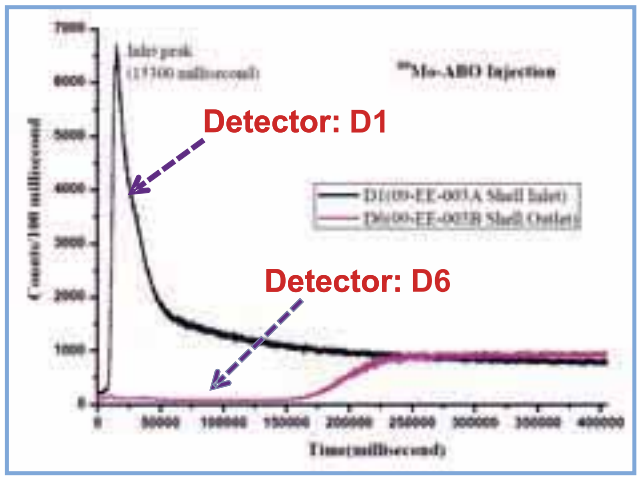

Fig.4: Detector response curve of D1 (shell inlet) and D6 (shell outlet)

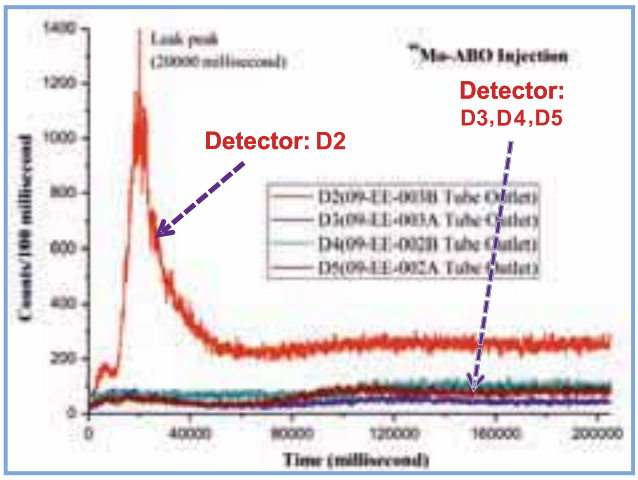

Fig.5: Detector response curve of D2, D3, D4 and D5 showing leak peak in the 09-EE-003B

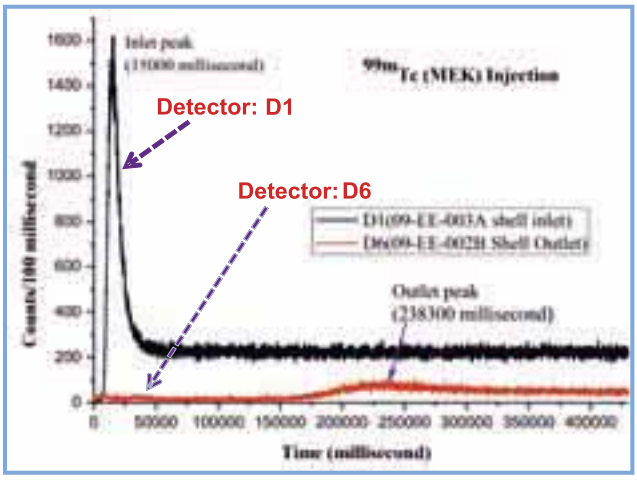

Fig.6: Detector response D1 (curve of shell inlet) and D6 (shell outlet)

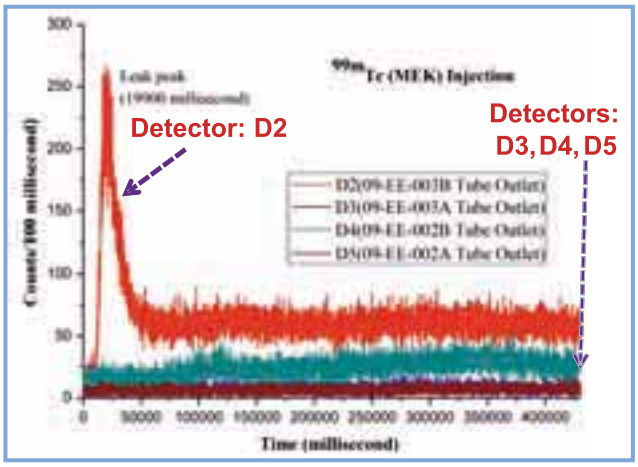

Fig.7: Detector response curves of D2, D3, D4 and D5 located at tube outlets of the heat exchangers showing leak peak in the 09-EE-003B

curve (Fig. 4) of detector D1 shows the instantaneous entry of the radiotracer into the shell side of heat exchanger 09-EE-003A. The time response curve of detector D6 (Fig. 4) shows the exit of the radiotracer from the shell outlet of heat exchanger 09-EE-002B. The output curve of D6 is stabilized after attaining a maximum value which indicates the adsorption of the radiotracer nearby the outlet pipe. Time response curves of the detectors D2, D3, D4 and D5 are shown in Fig.5. The peak observed at a time of 20000 millisecond in the time response curve of detector D2 corresponds to the leakage in the heat exchanger 09-EE-003B. The difference between inlet peak & leak peak was around 4.7 s. However, no peak was observed in the response curve of D3, D4 and D5 in the heat exchangers 09-EE-003A, 09-EE-002A/2B respectively. A slight rise of the signal was observed in all the detectors at around 80000 millisecond which may be attributed to the cross-detection of radiotracer travelling in shell side of adjacent heat exchangers. However, this rise is insignificant as compared to the leak peak observed.

A second radiotracer injection was carried out by injecting ^{99m}Tc dissolved in diesel. The peak observed at a time of 15000 millisecond in the response curve of detector D1 (Fig. 6) shows the instantaneous entry of the radiotracer in to the shell side of heat exchanger 09-EE-003A. The peak observed at a time of 238300 millisecond in the response curve of detector D6 (Fig. 6) shows the exit of the radiotracer from the shell side of heat exchanger 09-EE-002B, with the approximate residence time of the radiotracer in the system being 223 seconds. Fig.7 shows the response of the detectors D2, D3, D4 and D5 placed at the tube outlets of the all the heat exchangers. Appearance of the peak at a time of 19900 millisecond in the time response curve of detector D2 indicates the leakage in the heat exchanger 09-EE-003B. The difference between inlet peak & leak peak was around 4.9 s. Time response curve of the detector D3, D4 and D5 shows absence of any leakage in the heat exchangers 09-EE-003A, 09-EE-002A/2B respectively.

Conclusions

Two radiotracers based on ^{99}Mo and ^{99m}Tc radioisotopes, suitable for mixing with diesel, were successfully prepared and used for industrial application. In DHDT unit of a leading petroleum refinery, ^{99}Mo radiotracer in the form of ^{99}Mo-ABO complex was injected to identify the leaky heat exchanger from a set of the four heat exchangers in series. The radiotracer investigation with ^{99}Mo based radiotracer indicates the leakage in heat exchanger 09-EE-003B.The results were replicated by using the radiotracer ^{99m}Tc in organic phase, indicating the reproducibility of the results and utility of ^{99}Mo-ABO complex radiotracer for such studies.^{99}Mo based radiotracer was found advantageous over ^{99m}Tc due to its high gamma energy and more penetration through the pipe walls.

References

1. International Atomic Energy Agency (IAEA) Guidebook on radioisotope tracers in industry, Technical reports series No. 316, Vienna, Austria (1990).

2. Samantray, JS., Sunil Goswami, Sharma, VK., Jayshree Biswal, Pant, HJ. "Leak detection in a high-pressure heat exchanger in a refinery using radiotracer technique". J. Radioanal. &Nucl. Chem. 302/2 (2014) 979-982.

3. International Atomic Energy Agency (IAEA) "Training course series No. 38, Guidebook on leak detection in heat exchangers and underground pipelines using radiotracers", Vienna, Austria (2009).

4. Charlton JS. "Radioisotope Techniques for Problem Solving in Industrial Process Plants", Leonard Hill (Eds.), Glasgow, London (1986).

5. ThýnJ. "Radioisotope Techniques for Process Optimization, Isotope praxis Isotopes", In: Environmental and Health Studies 25/4 (1989) 144-151.

6. Pant, HJ., Kundu, A., Nigam, K. "Radiotracer applications in Chemical Process Industry". Reviews in Chemical Engineering 17/3 (2011) 165-252.

7. "Radiotracer residence time distribution method for industrial and environmental applications", IAEA Training Course Series No. 31, Vienna (2008).

8. "Chapter I: Bromine Isotopes. Decay Schemes of Br-80m and Br-82 and Their Properties for Impulse Counting and Autoradiography". Acta Radiologica, 53:sup190 (1960)15-22.

9. McAuley, R., Lull, R. & Ice, R. "Bromine-82 contamination in fission product ^{99m}Tc-generator eluate". Eur. J. Nucl. Med., 10 (1985) 60-62.

10. National Association for Applications of Radioisotopes and Radiation in Industry, Mumbai (India) Ramamoorthy, N.Ananthakrishnan, M., Ananthakrishnan, M., & Nandakumar, A.N. (Eds.). (2001). Proceedings of NAARRI international conference on applications of radioisotopes and radiation technology in the 21st century. India: National Association for Applications of Radioisotopes and Radiation in Industry.

11. Thýn J. "Chemical process analysis with nuclear technique", The International Journal of Applied Radiation and Isotopes 32/10 (1981) 733-746.

12. Mohd Yunos M A S, S A, Sipaun S M. "Industrial radiotracer application in flow rate measurement and flowmeter calibration using ^{99m}Tc and ^{198}Au nanoparticles radioisotope", Applied Radiation and Isotopes 143 **(2019)** 24-28.

13. Ram, R., Chakravarty, R., Pamale, Y., Dash, A. & Venkatesh, M. "An Alumina based ^{99}Mo-^{99m}Tc Generator to produce ^{99m}Tc in Organic medium suitable for Industrial Radiotracer Applications". Chromatographia. 69 (2009) 497-501. 10.1365/s10337-008-0931-9.

14. Noronha, O P D. "Solvent Extraction Technology of ^{99}Mo-^{99m}Tc Generator System 1. An Indian Experience: Process Design Considerations, Isotope praxis Isotopes", In: Environmental and Health Studies 22/2 (1986) 53-57.

15. Hwang, D S., Choung, W M., Kim, Y K., Park, J H., Park, S J. "Separation of ^{99}Mo from a simulated fission product solution by precipitation with -benzoin oxime". J. Radioanal. Nucl. Chem., 254 (2002) 255-262.

Present Status of High Intensity Cobalt-60 Sealed Sources in India

T. M Ashraf, S. Anwer Tariq, S.P Gupta, P. Baral, D. Paul & R. Sahu

Regional Centre, BRIT/ Rajasthan Atomic Power Plant Cobalt Facility (RAPPCOF), Kota.

(Corresponding Author: ashraf.t@britatom.gov.in)

Abstract

The application of ionizing radiation and radiation technology in healthcare, industry, agriculture and research is one of the most significant peaceful uses of nuclear energy, along with the nuclear power generation. Radiation processing of medical supplies & food and spices, using gamma rays is the most popular and beneficial application, just next to the teletherapy treatments of cancer. High intensity Cobalt-60 (^{60}Co) sealed sources are widely used for radiation processing considering the energy of emitted photons, half-life and means of production. Board of Radiation and Isotope Technology (BRIT), a unit of Department of Atomic Energy (DAE), is the only radiation source supplier in India, which undertakes the fabrication of ^{60}Co, its supply and post supply management, in a systematic and safe manner. BRIT supplies sealed sources, as per the demand in the country and abroad, with the ^{60}Co that is produced in various Indian PHWR type power reactors as a byproduct of neutron regulation. This paper describes the present status of ^{60}Co sealed source in the country.

Introduction

Ionizing radiation and radiation technology applications in the fields of healthcare industry, agriculture and research, are one of the most significant peaceful uses of nuclear energy, along with the nuclear power generation. Early realization of importance of radioisotopes and radiation technology for societal benefits and national development by the Department of Atomic Energy (DAE), resulted in development and setting up of infrastructural facilities in the country for harnessing the benefits of nuclear technology for the benefit of society. Accordingly, the Board of Radiation and Isotope Technology (BRIT) was carved out of Bhabha Atomic Research Centre (BARC) in the year 1989, as an independent unit under DAE with the intention of popularizing this technology for welfare of the people in the country.

Sealed radioactive sources are widely used for beneficial purposes throughout the world in industry and in medicine. The nuclear reactor produced high intensity ^{60}Co sources are being used for Cancer Teletherapy treatment, is a well-known fact. The radiation processing ^{60}Co gamma rays is the most popular and beneficial uses next to the teletherapy treatments of cancer, considering the energy of emitted photons, half-life and means of production, etc. There are plenty of other applications in which high intensity ^{60}Co sealed sources were effectively used globally. This requires ^{60}Co sealed sources

with activity greater than thousands of Curies. ^{60}Co is a synthetic radioactive isotope of cobalt with half-life of 5.27 years. It is produced artificially by neutron activation of the naturally occurring isotope ^{59}Co.

Isotope Group of BARC started its production in CIRUS in the early sixties. The Pressurized Heavy Water Reactors (PHWR) programme of Department of Atomic Energy for power production created an opportunity to take up production of ^{60}Co on large scale. Rajasthan Atomic Power Project (RAPP) was the first unit in the series of PHWRs. RAPP Cobalt Facility (RAPPCOF) was established within the exclusive zone of RAPP in the early seventies to coincide with the commissioning of first unit with annual production capacity of 2.0 Million Curies of ^{60}Co activity. Cobalt facility is engaged in cutting and recovery of ^{60}Co activity from adjuster rods of various power reactors in the country, since its inception. It started fabricating various sealed sources since the Year 2006, when the facility was augmented. During the last four decades, RAPPCOF progressed in leaps and bound, today it is the only facility in the country with a complete production cycle, where all works from receiving of cobalt adjusters from reactors to fabrication, supply and post-supply jobs of sealed sources are carried out. This is also the nodal facility catering the demand of sealed sources for all industrial irradiators across the country.

RAPPCOF crossed the milestone by processing 2.7 Million Curies of ^{60}Co in the Year 2013, 4.0 Million Curies in the Year 2018, and could process 6.7 Million Curies in the Calendar Year 2021. In addition to the supply of industrial irradiator sources, RAPPCOF is engaged in fabrication of ^{60}Co Teletherapy Sources (CTS) for the treatment of cancer, by successfully fabricating the CTS with greater than 200 RMM using indigenous activity since the Year 2013 onwards. Now, our Country is not importing any high intensity ^{60}Co sealed sources, which is used for radiation processing and Teletherapy, and, on the contrary BRIT has started exporting the sealed sources, only after meeting the demands in the country. This has, not only led to have a recognition of BRIT in a global market, but also is bringing foreign exchange revenue back to our Country.

Materials & Methods

^{60}Co is a synthetic radioactive isotope of cobalt with a half-life of 5.27 years. It is produced artificially by neutron activation of the naturally occurring isotope ^{59}Co. PHWR type power reactors use adjuster rods and regulating rods based on Cobalt for xenon override and control of reactivity in their operations (Fig.1). Cobalt is produced in two forms, i.e. 6mm dia x 25 mm long cobalt slugs and 1mm dia x 1mm long nickel-plated pieces called pellets doubly encapsulataed in Zircalloy capsules as per the specific activity (Ci/g) requirement of sealed sources. For example, the low specific activity (~60 Ci/g) ^{60}Co would suffice for radiation processing applications, whereas very high specific activity (HSA^{60}Co) (>200 Ci/g), is needed for teletherapy applications.

The activated ^{60}Co absorber rods are transported after certain period of irradiation in Nuclear Power Plants to

RAPPCOF where the further processing and fabrication of high intensity sealed sources like Multi-Purpose Gamma Irradiator Sources and ^{60}Co teletherapy Sources (CTS) are fabricated. High intensity ^{60}Co sealed sources are used in Teletherapy of Cancer treatment, radiation processing applications including sterilization of medical products, Post-harvest preservation of food grains, meat, fruits and vegetables, Sludge hygienisation, etc.

Fig. 1: ^{59}Co Absorber rod: Pellets, slugs, sub-Assemblies constitute Absorber rod

The specific activity of ^{60}Co obtained from Indian PHWR was < 180 Ci/g till the year 2010. CTS requires > 200 Ci/g specific activity to be fabricated and it was impossible to fabricate CTS with indigenous activity. The importing of HSA ^{60}Co for CTS ended up in very high cost for the teletherapy source. The scenario changed after India-United States Civil Nuclear Agreement (123 agreement), which ensured the availability of nuclear fuel for power generation in India and triggered the production of indigenous HSA ^{60}Co. From 2013 onwards, we have sufficient quantities of indigenous HSA ^{60}Co,which are essential for medical application, as well as medium specific activity ^{60}Co, which is required for Multi-Purpose Gamma Irradiators (Fig. 2).

Fig. 2: Sealed sources: Cobalt-60 Teletherapy Sources (CTS), W-91 and BC-188 model Multi-Purpose Gamma Irradiator Sources

Results and Discussion

The use of ^{60}Co for teletherapy application has significantly decreased across the globe due to the availability of better technology, still the scope of cost-effective ^{60}Co exists, mainly for those who can't afford the expensive technologies. But, in the case of radiation processing application, the trend is reverse. The commercial use of gamma radiation processing is now well entrenched. With increasing experience and confidence in the technology, more applications are investigated and added, and more facilities are being built in India and abroad. There was only one irradiation plant in the whole of South Asia in 1974, operating only for sterilisation application, which was ISOMED under DAE and today around 30 Multi-Purpose Gamma Irradiators are operating in India mostly under private partnership and around 200 irradiators across the globe. This leads to a huge demand for ^{60}Co 'High-intensity' sealed sources in domestic as well as in global market.

The demand of Multipurpose Gamma Irradiator Sources increased many folds in recent years. An increase from one Million Curies to more than six Million Curies, and, to a projected demand of eight Million Curies in this calendar year (2022), is expected. To cater this huge demand, Indian Source supplier, Board of Radiation and Isotope

Technology (BRIT), has increased their production capacity at RAPPCOF, and further expansion of the facility is underway to grab the global market, which is very huge. This gigantic demand is the outcome of combined demands in the country and abroad (Fig. 3).

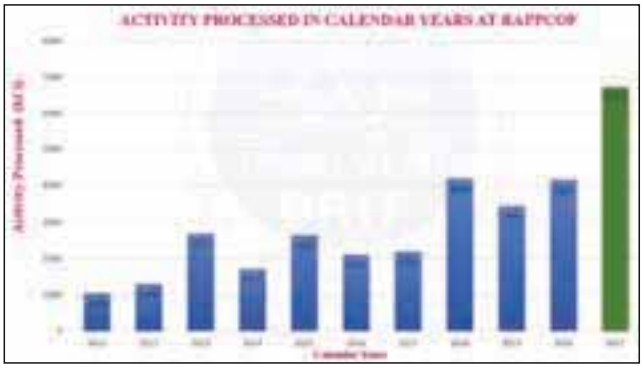

Fig. 3: Activity processed in Calendar year as per the demand at RAPPCOF

The leading ^{60}Co source supplier like **M/s. NORDION, M/s. REVISS, M/s. ROSATOM, etc.,** now depends on India, to meet their domestic demand. Apart from this, countries like Malaysia, Vietnam, Sri Lanka, etc. are some of the customers of (Indian produced) high-intensity Multipurpose Gamma Irradiator Sources.

Conclusion

The demand of ^{60}Co increased notably during last 10 years, due to the encouragement of private entrepreneurs to enter in the field of radiation processing. There are several numbers of irradiators operational in the various parts of the country and this number is growing up. These plants, which are coming up in different parts of the country with technical support from BRIT, are offering an alternative to traditional methods of sterilization and food preservation. The ^{60}Co contributes enormously to the health and wellbeing of a large proportion of the global population and has a positive economic, social and environmental impact that is sustainable for the future in this country. The benefits from the ionising radiation to society is greatly overbalance the risks. India is utilising every opportunity to grab the global ^{60}Co market, with full effort, by increasing the processing of ^{60}Co, as possible and by expanding the fabrication facility, as per the future demands.

Fig. 4: 1.0 Million curies of BC-188 model Multi-Purpose Gamma Irradiator Sealed sources being exported to M/s. Nordion (Canada) Inc. from RAPPCOF during 2022

Acknowledgement

The successful application of radiation technology in the industry is the result of the contribution of a large number of scientists and engineers from various units of DAE, who have worked tirelessly to master the technology. The efforts from Nuclear Power Corporation of India Limited (NPCIL) to timely provide ^{60}Co Adjuster/Absorber rods is acknowledgeable. At the facility, we are committed for judicious supply of sealed sources, to the end users, in a safe manner & strictly in compliance with Atomic Energy Regulatory Board (AERB) regulations, and will continue to contribute to the society.

References

1. Brochure of Gamma Irradiators for Radiation Processing by International Atomic Energy Agency (IAEA), Vienna, Austria.

2. Factsheet – Beneficial uses of ^{60}Co by International Irradiation Association (iia).

Production of Medically useful Radioisotopes and corresponding Radiopharmaceuticals in 30 MeV Cyclotron

[1]*Sankha Chattopadhyay*, [*]*Pradip Mukherjee*

[1]**Regional Centre, BRIT, VECC, MCF, Kolkata, 700094;**
[*]**Chief Executive, BRIT, Vashi Complex, Vashi, Navi Mumbai-400703**

(Corresponding author: sankha@vecc.gov.in)

Abstract

Cyclotrons are extensively used to produce radioisotopes for diagnostic and therapeutic use for cancer care. In India, the IBA Cyclone-30, 30MeV, 350μA proton cyclotron has been commissioned and made operational during September, 2018, for the production of radioisotopes / radiopharmaceuticals for medical application. The cyclotron has five beamlines, out of which three beamlines are dedicated for the production of radioisotopes for medical use. This cyclotron has the potential to produce SPECT (Single-Photon Emission Computed Tomography) Isotopes (^{67}Ga, ^{111}In, ^{123}I, ^{201}Tl etc.), PET (Positron Emission Tomography) isotopes (^{18}F, ^{68}Ga, ^{64}Cu, ^{89}Zr, ^{124}I, ^{68}Ge for ^{68}Ge-/^{68}Ga- Generator for in-situ production of ^{68}Ga, etc.) and therapeutic isotope like ^{103}Pd. Herein, the production of ^{18}F-FDG, ^{68}Ga-PSMA-11 and ^{201}TlCl radiopharmaceuticals using Cyclone-30 has been reported. The specification of the radiopharmaceuticals complies with norms of the regulatory bodies in India. Presently, India is importing long lived SPECT radioisotopes. The high cost of imported isotopes makes the treatment expensive. Indigenous production is going to be a boon to make the treatment cost more affordable.

Introduction

Currently, ^{18}F-FDG is considered as the most successful PET radiopharmaceutical. The advancement in synthesis and quality control of ^{18}F-FDG, together with its approval by the US FDA and the availability of reimbursement, are probably the main reasons for the flourish of clinical PET imaging. The labelled ^{18}F-FDG compound has a relatively short shelf life, which is dominated by the physical decay of ^{18}F with a half-life of 109.8 minutes, or slightly less than 2 hours. Still, this half-life is sufficiently long to allow the shipping of the compound to remote PET scanning facilities, in contrast to other medical radioisotopes like ^{11}C. In PET imaging, ^{18}F-FDG can be used for the assessment of glucose metabolism in the heart, lungs [1], and the brain. It is also used for imaging tumors in oncology, where a static ^{18}F-FDG PET scan is performed and the tumor ^{18}F-FDG uptake is analysed in terms of Standardized Uptake Value (SUV). ^{18}F-FDG is taken up by cells, phosphorylated by hexokinase (whose mitochondrial form is greatly elevated in rapidly growing malignant tumours) [2], and retained by tissues with high metabolic activity, such as, most types of malignant tumours. As a result, FDG-PET can be used for diagnosis,

staging, and monitoring treatment of cancers, particularly in Hodgkin's disease, non-Hodgkin lymphoma, colorectal cancer, breast cancer, melanoma, and lung cancer. It has also been approved for use in diagnosing Alzheimer's disease.

The SPECT isotope ^{201}Tl ($t_{1/2}$ = 73.06 hours) in the form of ^{201}TlCl is a diagnostic myocardial flow tracer to detect coronary artery disease and to assess myocardial viability, with an accuracy comparable to that of positron emission tomography. Other medical applications of the same include possible assessment of physiology, as a renal medullary imaging agent, and for tumor detection [3]. ^{201}TlCl has higher myocardial extraction fraction (85%) compare to ^{99m}Tc-MIBI (65%) and ^{99m}Tc-Tetrofosmin (60%). The lower myocardial extraction fraction of ^{99m}Tc-MIBI and ^{99m}Tc-Tetrofosmin results in underestimation of blood flow at high flow compared to ^{201}TlCl [4]. Clearance half-life is faster in case of ^{201}TlCl compare to ^{99m}Tc-MIBI and ^{99m}Tc-Tetrofosmin [5]. ^{201}Tl decays to stable Mercury-201 (^{201}Hg) nuclide via electron capture with the emission of mercury K-X-rays of 69 - 83 keV (90%) along with γ-rays of 135 keV and 167 keV in total abundance of 10%. ^{201}Tl is produced in Cyclone-30 using solid target via ^{203}Tl(p,3n)^{201}Pb $\rightarrow$ ^{201}Tl nuclear reaction utilizing a proton (energy: 28MeV) beam current of 50μA for up to 6-8h. The potential radionuclidic impurities in Thallium-201 produced with during the above nuclear reaction are Thallium-200 (^{200}Tl, $t_{1/2}$ = 26 h), Thallium-202 (^{202}Tl, $t_{1/2}$ = 12.2 d) and Lead-203 (^{203}Pb, $t_{1/2}$ = 52 h). However, the percentage for formation of ^{200}Tl, ^{202}Tl and ^{203}Pb can be controlled by optimizing the incident proton energy (28 MeV) on the target during irradiation and giving an optimum decay time of 32 h for ^{201}Pb to ^{201}Tl [6]. The allowed limits for ^{200}Tl, ^{202}Tl and ^{203}Pb were 0.6%, 1.2% and 0.2% expressed as a percentage of ^{201}Tl injection activity at calibration date and time [7]. There are many approaches that addresses the wet separation of ^{201}Pb from ^{203}Tl and ^{201}Tl from ^{201}Pb from a dissolved solid target, typically ending with ^{201}TlCl as the product. Such approaches include ion exchange resin chromatography and solvent/solvent extraction [8]. Ion exchange column chromatography and solvent extraction methods have been employed by us for radiochemical separation and purification of ^{201}Tl from dissolved solid target. We, herein, report a semi-automated production of curie level, pharmaceutical grade ^{201}TlCl using IBA Chemistry module.

Gallium-68 (^{68}Ga, $t_{1/2}$ = 67.8 min) possesses great potential in nuclear medicine [9,10] being extensively used in labelling of biomolecules like somatostatin and PSMA inhibitor analogues [11,12,13,14]. ^{68}Ga decays to stable ^{68}Zn nuclide via electron capture (11%) and positron decay (89%) and is generally produced via ^{68}Ge/^{68}Ga generators [15,9]. An alternative method to produce ^{68}Ga is by cyclotron using high enriched ^{68}Zn via the ^{68}Zn(p,n)^{68}Ga reaction [16,17,18]. There are many approaches that address the wet separation of ^{68}Ga and ^{68}Zn from a dissolved solid target, typically ending with [^{68}Ga]$GaCl_3$ as the product. Such approaches include solid phase extraction, solvent extraction, and precipitation [19,20]. Ion Exchange column chromatography and solvent extraction methods have been employed by us for radiochemical separation and purification of ^{68}Ga from dissolved solid target. Due to

the increasing demand for various ^{68}Ga based radiopharmaceuticals production and applications entering clinical trials worldwide, there is a need to produce large quantity of ^{68}Ga. Hence, $^{68}GaCl_3$ is produced on medium energy cyclotron via the $^{68}Zn(p,n)^{68}Ga$ reaction which is useful for production of large quantity of ^{68}Ga. The starting material is a solid target in the form of a target plate, since solid target will always have a higher concentration of zinc, which leads to significantly higher yields. Furthermore, the ^{68}Ga must be separated from the bulk parent ^{68}Zn isotope and purified to remove any unwanted metal contaminants. The end product obtained is $^{68}GaCl_3$, which is similar to the eluate obtained from the $^{68}Ge/^{68}Ga$ generator, is then used as a solution for radiolabelling to prepare ^{68}Ga-based diagnostic radiopharmaceuticals like ^{68}Ga-PSMA-11, ^{68}Ga-DOTA-TATE. Currently, [^{68}Ga]Ga-PSMA-11 (Glu-NH-CO-Lys-(Ahx)-[[^{68}Ga]Ga-HBED-CC] (HBED CC: N,N'-Bis(2-hydroxy-5-(ethylene-betacarboxy) benzyl ethylenediamine N,N'-diacetic acid) is among the most widely used agents for prostate cancer PET/CT imaging. Prostate cancer is one of the leading causes of morbidity and death in men in the western world, and the second most common cancer in men worldwide [21]. We, herein, report a semi-automated production of Curie level, pharmaceutical grade [^{68}Ga]$GaCl_3$ radiochemical and [^{68}Ga]Ga-PSMA-11 radiopharmaceutical, using IBA Chemistry module.

Experimental

Production of Different Radioisotopes and Radiopharmaceuticals

[1]. Production of ^{18}F-FDG Radiopharmaceutical using IBA-SYNTHERA Module

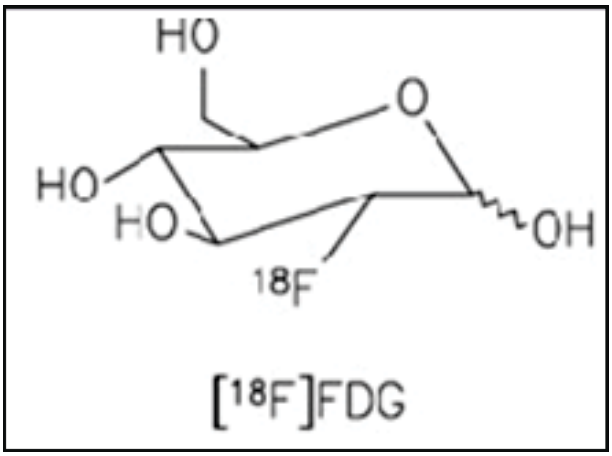

Fig. 1: Structure of ^{18}F-FDG

Production of ^{18}F from ^{18}O Water and Synthesis of ^{18}F-FDG

[^{18}F]fluoride ion/[^{18}O]water was transferred from target to chemistry module, following which the synthesis of ^{18}F-FDG (Fig. 1) was carried out using automated, closed loop and computer-controlled IBA synthera module (Fig. 2) inside Comecer make Hotcells (75 mm Pb thickness wall). ABX, Germany reagents and ancillary kits along with IFP (Integrated Fluidic Processor) are utilized in the IBA Synthera module for the synthesis and purification of ^{18}F-FDG (Fig. 3).

The ^{18}F is produced in the cyclotron by irradiation of $H_2{}^{18}O$ (97% enriched) [$^{18}O(p,n)^{18}F$] using 18 MeV proton beam

Fig. 2: IBA-SYNTHERA Module

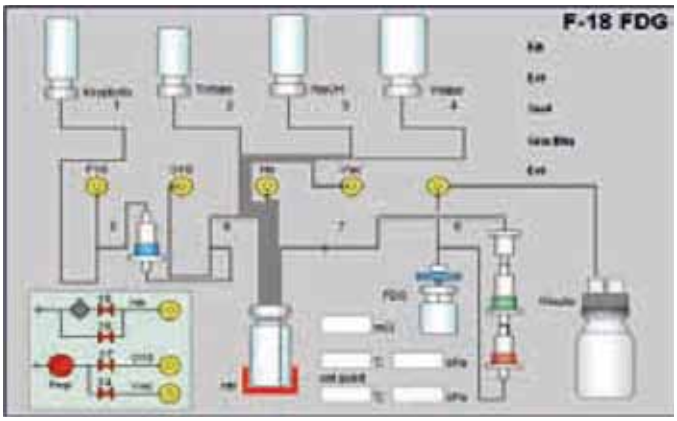

Fig. 3: ^{18}F-FDG Synthesis Flow Diagram

(35-45 A current) for 30 min to 2 hours (Fig. 4 and Fig. 5). The dispensing of the product is carried out using TIMOTHEO-LT dispensing module inside Comecer dispensing Hot cell having ISO Class A environment. The final ^{18}F-FDG product obtained from IBA Synthera synthesis module is collected in 30 ml sterile glass vial (supplied by ABX Germany) containing 0.68 ml of 14.6% sodium chloride (inactive ingredient) to make the final solution isotonic, in the dispensing hotcells. The production yield of ^{18}F-FDG varied from 65-70% (without decay correction). A 0.5 ml of sample from each FDG batch was taken in a sterile vial for Q. C. analysis. The physico-chemical and bio quality control tests were performed as per USP specifications with satisfactory results.

[2]. Production of ^{201}Tl in the form of ^{201}TlCl, suitable for diagnostic uses in patients

Irradiation of the target

^{201}Tl has been produced on medium energy cyclotron, Cyclone-30, via the ^{203}Tl(p,3n)^{201}Pb $\rightarrow$ ^{201}Tl nuclear reaction. The starting material is a solid target in the form of a target plate electrodeposited with enriched Thallium-203 (Fig. 6 and Fig. 7), which leads to significantly higher yields. Further, the ^{201}Tl must be separated from the bulk parent ^{203}Tl and ^{201}Pb isotope and purified to remove any unwanted metal contaminants. The end product has been supplied as a ready-to-use sterile, pyrogen free, isotonic aqueous solution of radioactive Thallium-201 (^{201}Tl) in the form

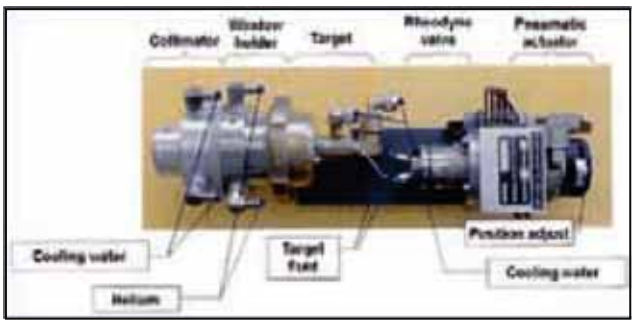

Fig. 4: Water Target for the Production of ^{18}F

Fig. 5: Conical shaped Niobium cavity for ^{18}O water

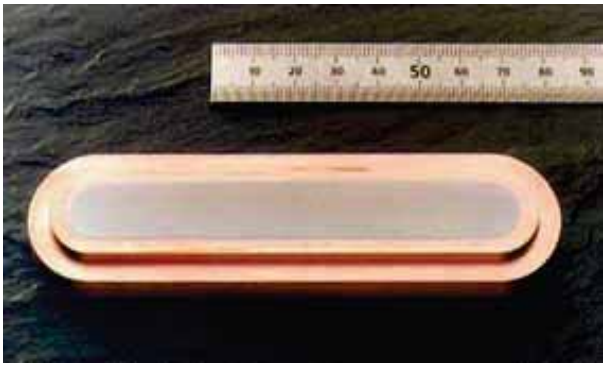

Fig. 6: ^{203}Tl Target

Fig. 7: Electrodeposition vessel

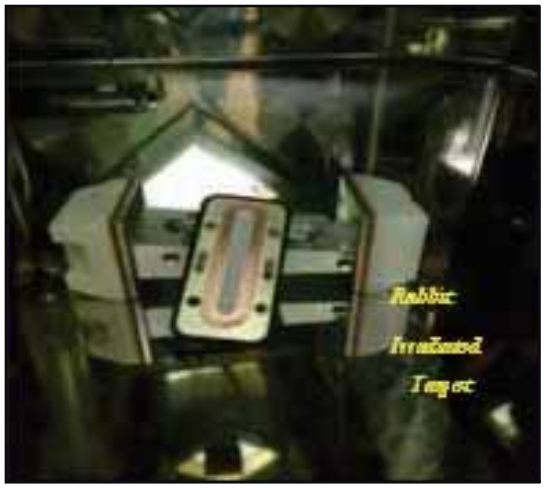

Fig. 8: Irradiated target system received in the receiving Hot cell.

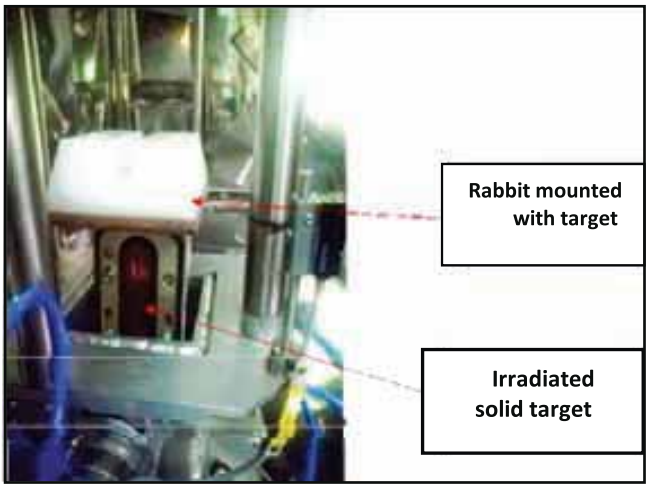

Fig. 9: Irradiated Enriched ^{203}Tl Target with Rabbit System in Receiving Hot cell

of thallous chloride solution for intravenous administration. Irradiations of the electrodeposited (~ 74 - 75 μm) ^{203}Tl targets were carried out with the 28MeV proton beam energy and 50μA beam current for up to 6-8h (n = 6) at 6° angle. During the irradiation the target assembly (Fig. 8 and Fig. 9) was water cooled with a flow rate of 9 liter/min. Beam current/charge deposited on the target was monitored with a current integrator.

Dissolution of the irradiated thallium target and separation of ^{201}Tl from ^{201}Pb

The original script for the ^{201}Tl chemistry-1 and chemistry-2 was supplied for production of [^{201}Tl]TlCl and thus required modifications, while working on our system (Fig. 10 and Fig. 11).

Chemistry-I: The irradiated target was dissolved in 25 ml of 0.7 N HNO_3 (containing 100 mg $Pb(NO_3)_2$). ^{201}Pb was precipitated as $^{201}PbSO_4$ by using 10 ml of 3.6 N H_2SO_4. The first dissolution of $^{201}PbSO_4$ was carried out with 10 ml of 0.1 M Na_2EDTA (pH ~ 9.0), while second dissolution was carried out with 10 ml of 0.1 M Na_2EDTA (pH ~ 5.4). $^{203}Tl^{3+}$ was reduced to $^{203}Tl^{+}$ by bubbling SO_2 gas. Ion Exchange Chromatography using Dowex 50W-X8 resin (100-200 mesh, H^+ form) was employed to remove co-precipitated $^{203}Tl^{+}$. Cation exchange chromatography was employed to adsorb $^{203}Tl^{+}$ in the

column while the ^{201}Pb-EDTA complex was collected in column eluate. ^{201}Pb-EDTA^{2-} complex was stored for 32 h for decay of $^{201}Pb^{2+}$ either to $^{201}Tl^{3+}$ or $^{201}Tl^{+}$.

Chemistry-II: Post 32 h decay, $^{201}Pb^{2+}$ (in the form of ^{201}Pb-EDTA mother solution) was converted to either $^{201}Tl^{3+}$ or $^{201}Tl^{+}$. The reduction of $^{201}Tl^{3+}$ to $^{201}Tl^{+}$ was carried out by bubbling SO_2 gas through the mother Pb-EDTA solution until a pH ~ 3 is attained. Post reduction, the pH of reduced $^{201}Tl^{+}$ in mother Pb-EDTA solution was adjusted to ~ 5.4 by using 1N NaOH. The mother Pb-EDTA solution containing $^{201}Tl^{+}$ was passed through Dowex 50W-X8 resin (100-200 mesh, H^+ form) chromatographic column. $^{201}Tl^{+}$ was adsorbed in the column while Pb-EDTA was collected as eluate in waste flask. The adsorbed $^{201}Tl^{+}$ was eluted from cation exchange chromatographic column using 15 ml of 6 N HCl. Further $^{201}Tl^{+}$ was oxidized to $^{201}Tl^{3+}$ using ozone. Solvent extraction of $^{201}Tl^{3+}$ from aqueous phase (HCl) to organic phase (DIPE) was carried out utilizing 20 ml DIPE (DIPE saturated with 6 N HCl). Reduction of $^{201}Tl^{3+}$ to $^{201}Tl^{+}$ was carried out by SO_2 gas in aqueous phase (0.005N HCl). Post reduction, $^{201}Tl^{+}$ was back extracted into 20 ml of 0.005N HCl. After successful removal of DIPE from aqueous phase, finally ^{201}TlCl ($^{201}Tl^{+}$ form, in 0.005N HCl) was collected. pH of ^{201}TlCl was adjusted to 6 - 7 using 1N NaOH and was diluted with 0.9% NaCl. ^{201}TlCl (in 0.9% NaCl) was filtered with sterile pyrogen free 0.20 μm PES membrane syringe filter. ^{201}TlCl ($^{201}Tl^{+}$ form) solution obtained was assayed for radioactive concentration and suitable activity was dispensed into sterile pyrogen free glass vials for supply.

The entire operation was carried out in aseptic environment using ultrapure grade chemicals and sterile and pyrogen-free glassware to ensure the purity (radionuclide, radiochemical and chemical), sterility and apyrogenicity of the product. The physicochemical quality control and BET assay was completed prior to supply of the product. Sterility was initiated within the same day of production. Following the revised configurations and the designed steps, the script was accordingly modified. The whole process of chemical separation and purification has been carried out in GMP certified hot cell and semi-automated radiochemistry module under aseptic environment for efficient, rapid and easy handling.

Fig. 10: Thallium Chemistry hot cell with Tl-chemistry module

[3]. Indigenous module for $^{68}GaCl_3$ radiochemical and ^{68}Ga-PSMA-11 radiopharmaceutical synthesis

Irradiation of the target

Irradiations of the electrodeposited (~ 94.5 – 95.5 μm) ^{68}Zn targets (Fig. 12) were carried out with the 15MeV proton beam of up to 60μA for 25 minutes (n = 6) at 6° angle. During the irradiation, the target assembly was water cooled with a flow rate of 9 liter/min. Beam current/charge deposited on the target was monitored with a current integrator.

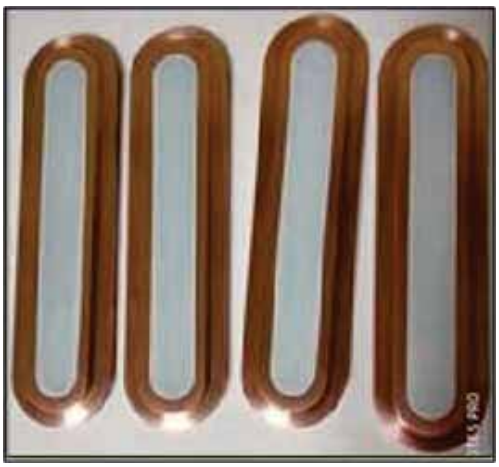

Fig. 12: Electroplated ^{68}Zn targets

Dissolution of the irradiated gallium target and separation of ^{68}Ga from ^{68}Zn

The original script for the ^{67}Ga chemistry was supplied by VUB for production of ^{67}Ga radiochemical and thus required modifications while working on our system. Beam energy was accordingly adjusted to obtain ^{68}Ga in Curie quantity

Production of $^{68}GaCl_3$ radiochemical

Irradiated target was placed in the dissolution unit of automated

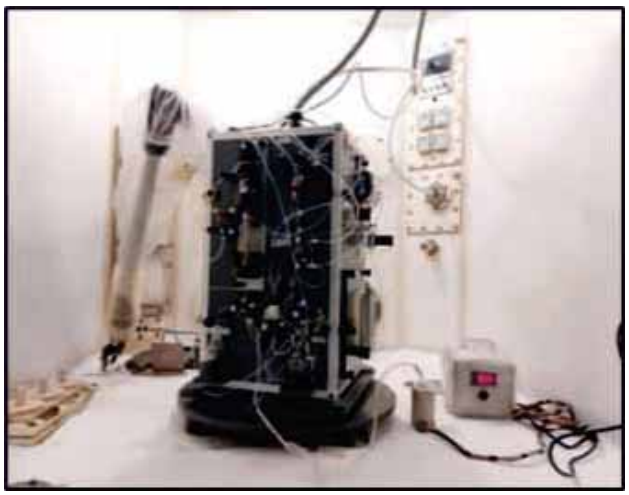

Fig. 13. Module for $^{68}GaCl_3$ and ^{68}Ga-PSMA-11 synthesis

radiochemistry module (Fig. 13) using master-slave manipulator. It was then dissolved using 20 ml of 10 N HCl (containing 100 μL H_2O_2). The enriched ^{68}Zn and carrier free Ga rapidly dissolved in this medium. Upon complete dissolution of the target material, about ~ 10 mg of Cu from Cu backings was co-dissolved. Dowex 50W-X8 resin (100-200 mesh, H^+ form) was packed in column (dimension of column: 1.33 cm^2 internal cross section area x 6 cm height). The column was preconditioned with 40 ml of 9 N HCl at a flow-rate of 2.0 ml/min. Separation of ^{68}Ga from Cu and ^{68}Zn was carried out by cation exchange chromatography using preconditioned Dowex 50W-X8 resin column (100 - 200 mesh, H^+ form). Stripping solution was applied to the chromatographic column at a flow-rate of 1.7 ml / min. The ^{68}Ga is adsorbed quantitatively, while the Cu and ^{68}Zn pass into the storage flask (^{68}Zn recovery storage flask). Interstitial Zn and Cu was removed from the column with 25 ml of 9 N HCl. ^{68}Ga was eluted with 20 ml of 3.75 N HCl from the column and the eluate is collected in extractor present inside radiochemistry module. Concentration of

HCl was adjusted prior to extraction of ^{68}Ga in DIPE for optimum extraction. 7 N HCl is the optimum concentration of HCl for ^{68}Ga extraction from HCl into DIPE. In extractor (containing ^{68}Ga eluate), 20 ml of 10 N HCl was added so as the concentration of HCl increases from 3.75 N to 7 N. Solvent extraction of ^{68}Ga from HCl to DIPE takes place by introducing 15 ml DIPE (DIPE saturated with 7N HCl) to extractor. Both the layers {aqueous (HCl) and organic (DIPE)} were mixed by bubbling N_2 gas through the aqueous layer. Post separation of both the phases, the HCl layer was transferred to waste-flask inside the radiochemistry module.

Preparation of $^{68}GaCl_3$ radiochemical

Back extraction was performed with DIPE in extractor after addition of 10 - 20 ml of 0.005N HCl. Finally, 0.005 N HCl layers was collected in the $^{68}GaCl_3$ flask inside radiochemistry module, whereas DIPE phase was transferred to the waste flask inside the radiochemistry module. Traces of DIPE was removed from $^{68}GaCl_3$ solution present in the flask and homogenization of the content was carried out by bubbling N_2 through the solution for 5 minutes at 90°C.

Synthesis of ^{68}Ga-PSMA-11radio-pharmaceutical

Radiolabelling was performed by adding buffer + peptide (PSMA-11, 100 μg) mixture (3 ml) to the reaction vial and heating for 10 mins at 95°C. 3 ml water for injection was added to the reaction vial. The mixture was passed through C-18 column and the waste was collected in the waste vial. 3 ml water for injection was again added to wash the C-18 column; collected in the waste vial. ^{68}Ga-PSMA-11 was eluted from the C-18 column using 3 ml 50% (v/v) EtOH and collected in the product vial containing 5 ml 0.9% saline. Column was washed with 2 ml water for injection and collected in the product vial.

Dispensing of ^{68}Ga-PSMA-11 radio-pharmaceutical

The resultant ^{68}Ga-PSMA-11 radiopharmaceutical solution was filtered using sterile pyrogen free 0.20 μm PES membrane syringe filter. Small aliquots (0.5 ml) of clinical grade ^{68}Ga-PSMA-11 solution was dispensed into sterile, pyrogen-free glass vials using the automatic dispensing system as per customer requirement. The glass vials were sealed with 25 Kgy irradiated, sterile, pyrogen-free bromobutyl rubber closures and crimped with aluminium caps (pre swabbed with 70% ethanol). The sealed glass vials were transferred to a cylindrical lead container (LP-30), surrounded by thermocol and placed inside an outer container made up of HDPE (TPPL-1) and sealed before being dispatched to hospitals.

The entire operation was carried out in an aseptic environment using ultrapure grade chemicals and sterile and pyrogen-free glassware to ensure the purity (radionuclide, radiochemical and chemical), sterility and apyrogenicity of the product. Physico-chemical and biological quality control of [^{68}Ga]Ga-PSMA-11 were optimized and carried out and they are in accordance with USP monograph, International Pharmacopeia and Indian Pharmacopeia. The clinical results from PET-CT Cardiac studies performed at Netaji Subhas Chandra Bose

Cancer Hospital, AMRI Hospitals (Dhakuria), Command Hospital (Eastern Command, Alipore Road), Kolkata add support to the use of our ^{68}Ga-PSMA-11 as a pharmaceutical grade diagnostic radiopharmaceutical.

Results

[1]. Quality Control Results of ^{18}F-FDG Radiopharmaceutical

The physicochemical quality control tests of ^{18}F-FDG were performed by checking appearance, pH, radiochemical purity (RCP), by either method A (HPLC) or method B (TLC). The HPLC system is more expensive and elaborate than the TLC system, radionuclide purity (RNP) using HPGe method.

The radioactivity assay i.e. yields determination and half-life estimation were performed in dose calibrator.

The presence of bacterial endotoxin in the ^{18}F-FDG were assayed by Charles River's Endosafe PTS (Portable Endotoxin Testing System).

The sterility testing for every individual batch of ^{18}F-FDG has been inoculated in both, fluid thioglycolate medium (FTM) and soybean casein digest medium (SCDM) within 30 hours of production at 37°C and 25°C respectively.

The residual solvent in ^{18}F-FDG i.e., ethanol and acetonitrile were estimated in Gas chromatography (GC).

The radiochemical purity of the ^{18}F-FDG has been found to be 100% by using TLC method (Fig. 14).

The radionuclidic purity was greater than 99.9% (determined by HPGe) (Fig. 15).

The presence of Kryptofix in the final product was found to be less than 22 μg/ml.

The residual solvent ethanol and ACN in ^{18}F-FDG were within the specified value (GC method) (Fig. 16).

HPLC study is required to know any radiochemical impurities like $^{18}F^-$, ^{18}F-FDM and ^{18}F-ClDG are present or not (Fig. 17 and Fig. 18).

The Bacterial endotoxin in ^{18}F-FDG was found <10 EU/ml determined by PTS method.

Each batch was evaluated for sterility test and each batch passes the sterility test.

PET-CT scan of ^{18}F-FDG was carried out in North City Centre, Kolkata (Fig. 19).

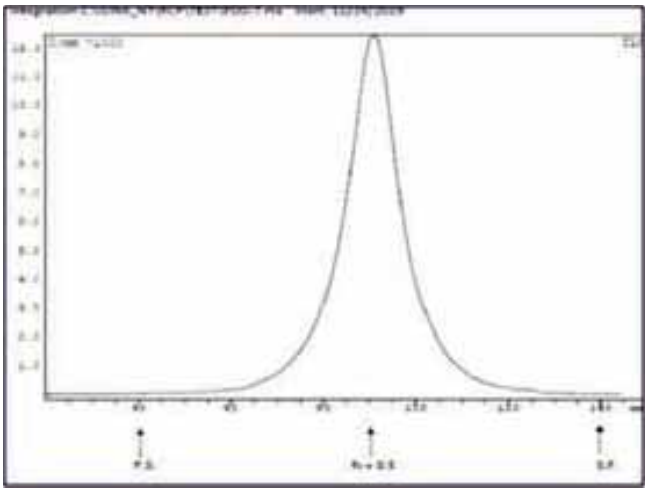

Fig. 14: TLC Spectra of ^{18}F-FDG

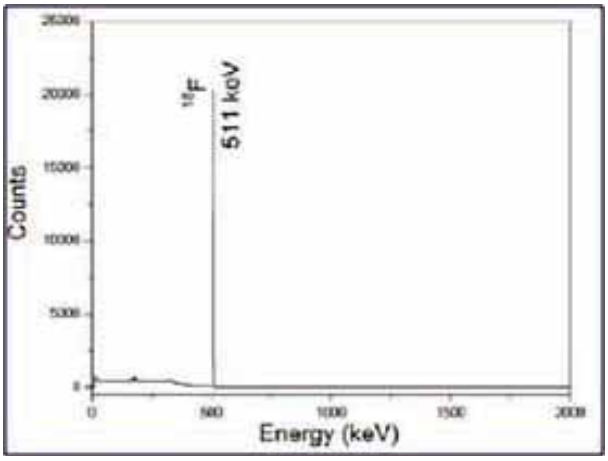

Fig. 15: HPGe Spectra of ^{18}F

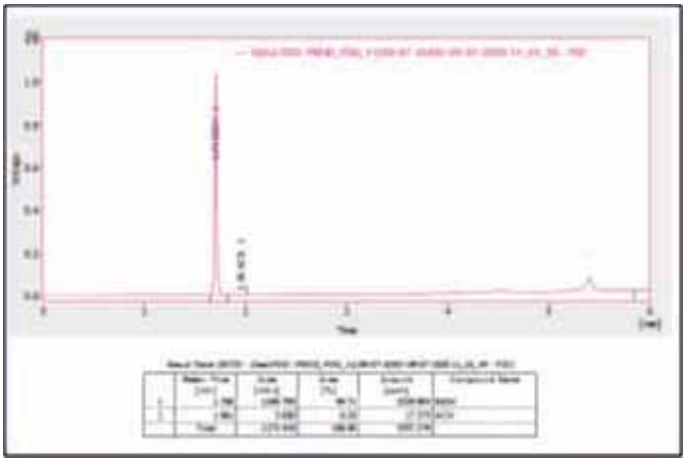

Fig. 16: GC Spectra of ^{18}F-FDG

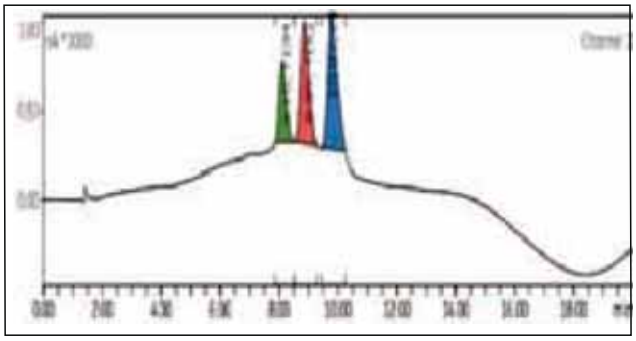

Fig. 17: HPLC Spectra of ^{18}F-FDG

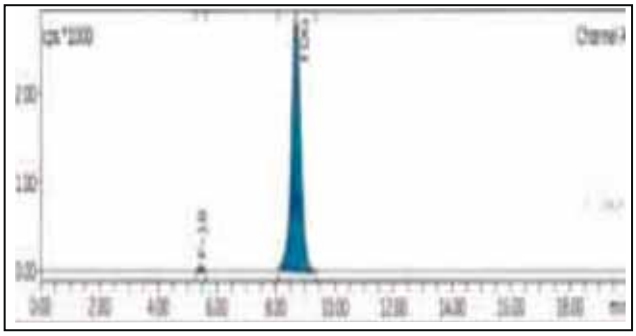

Fig. 17: HPLC Spectra of ^{18}F-FDG

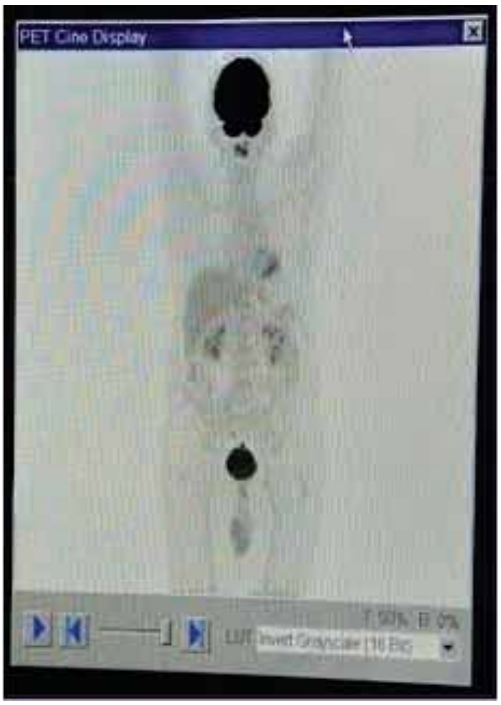

Fig. 19: PET-CT Scan of ^{18}F-FDG carried out in North City Centre, Kolkata

Overall Physicochemical and Biological Quality Control Tests Results of ^{18}F-FDG are shown in Table 1

Table 1: Physicochemical and Biological Quality Control Tests of ^{18}F-FDG

Batch No.	Appearance	pH	Half-life (min)	RC Purity (RCP)	RN Purity (RNP)	Kryptofix (<22 mg/mL)	Acetonitrile (ppm)	Ethanol (ppm)	BET Test (<10 EU/mL)	Sterility Test
1	Clear	6.5	109.1	100	99.9	Pass	17.88	1705.96	Pass	Pass
2	Clear	6.0	110.7	100	99.9	Pass	14.04	1756.94	Pass	Pass
3	Clear	6.0	109.9	100	99.9	Pass	18.21	1641.4	Pass	Pass
4	Clear	6.5	108.9	100	99.9	Pass	<5	1344.48	Pass	Pass
5	Clear	6.0	109.5	100	99.9	Pass	14.60	1481.3	Pass	Pass
6	Clear	6.5	109.8	100	99.9	Pass	15.59	1506.85	Pass	Pass

[2]. Quality Control Results of ^{201}TlCl Radiopharmaceutical

The radiochemical purity of ^{201}TlCl was 100% (PC method) (Fig. 20).

The metal content of ^{201}TlCl (Fe, Cu and Tl) were within the specified values.

The Bacterial Endotoxin in ^{201}TlCl was < 6 EU/ml (PTS method)

The residual solvent DIPE in ^{201}TlCl was within the specified value (GC method) (Fig. 21).

The radionuclidic purity of ^{201}Tl was > 99% (determined by HPGe) (Fig. 22).

Each batch were evaluated for sterility test and each batch passed the sterility test.

SPECT-CT scan of ^{201}TlCl was carried out in NH Rabindranath Tagore, International Institute of Cardiac Sciences, Kolkata (Fig. 23).

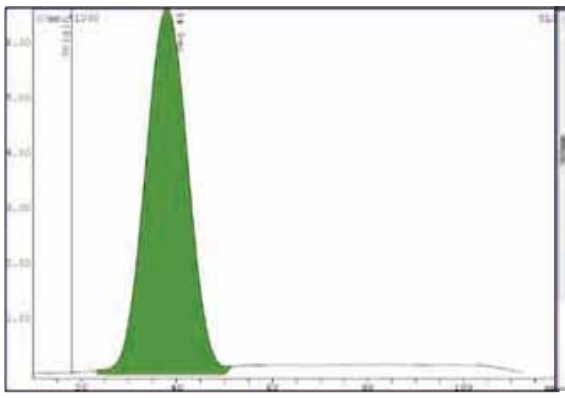

Fig. 20: PC Spectra of ^{201}TlCl

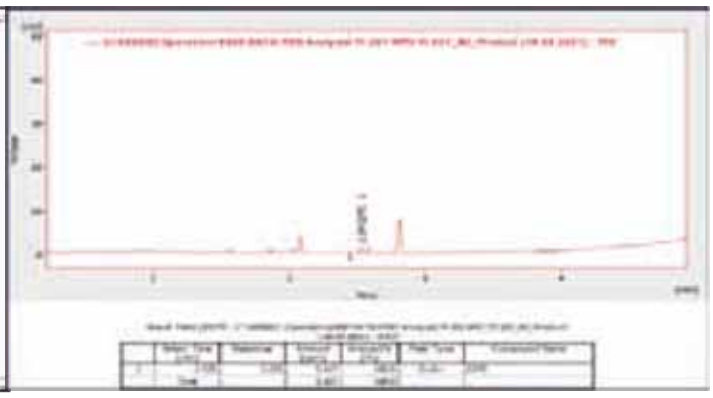

Fig. 21: GC Spectra of ^{201}TlCl

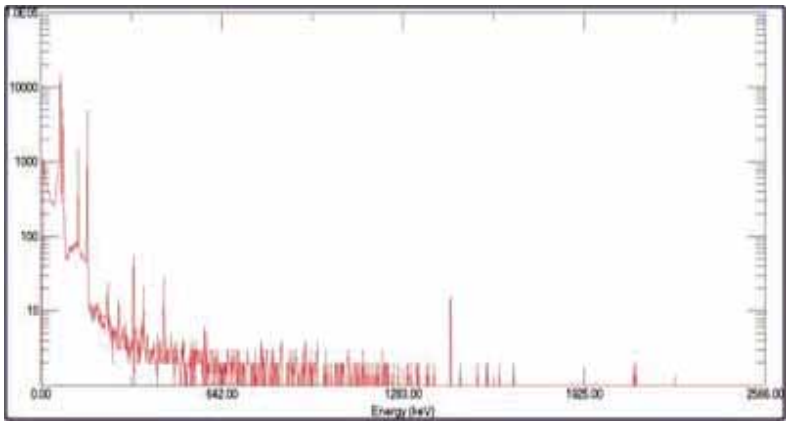

Fig. 22: HPGe Spectra of ^{201}TlCl

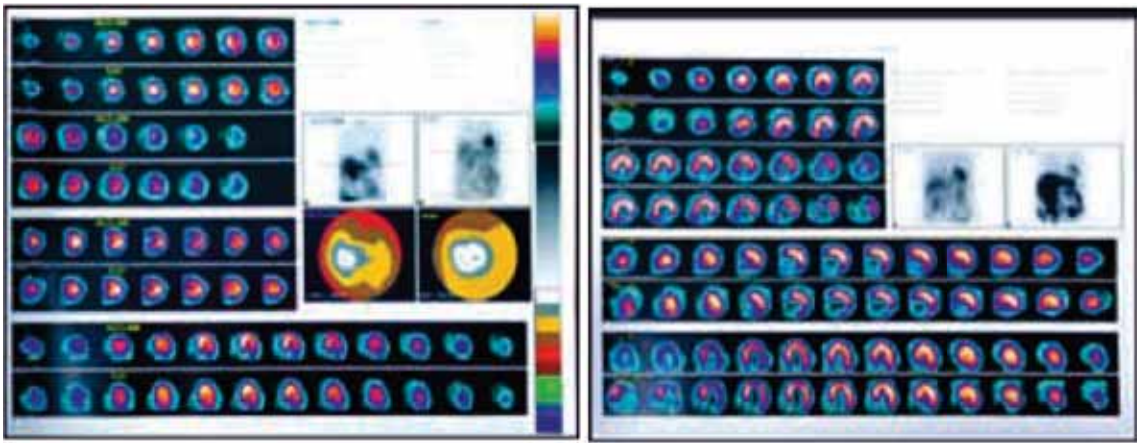

Fig. 23. Two cardiac studies (Rest-Stress on 18/12/2021 for ischemia evaluation and rest only for viability assessment on 20/12/2021) using GE Discovery 670DR SPECT-CT scanner in patients for suspected coronary artery disease evaluation: A comparison between ^{201}TlCl vs ^{99m}Tc-MIBI performed on same patients.

Overall Physicochemical and Biological Quality Control Tests Results of ^{201}TlCl are shown in Table 2.

Table 1: Physicochemical and Biological Quality Control Tests of ^{201}TlCl

Batch No.	Appearance	pH	Half-life (hrs)	RC Purity (RCP) (%)	RN Purity (RNP) (%)	Fe (Fe^{2+}) (µg/mL)	Cu (Cu^{2+}) (µg/mL)	Tl (Tl^{+}) (µg/mL)	BET Test (<6 EU/mL)	Sterility Test
1	Clear	5.0	73.68	100	99.8	< 3	BDL	< 2	Pass	Pass
2	Clear	6.0	73.2	100	99.9	< 3	BDL	< 2	Pass	Pass
3	Clear	5.0	73.1	100	99.9	< 3	BDL	< 2	Pass	Pass
4	Clear	6.5	73.6	100	99.8	< 3	BDL	< 2	Pass	Pass
5	Clear	5.0	73.1	100	99.8	< 3	BDL	< 2	Pass	Pass
6	Clear	5.5	73.2	100	99.8	< 3	BDL	< 2	Pass	Pass

BDL – Below Detectable Limit

[3]. Quality Control Results of $^{68}GaCl_3$ Radiochemical and [^{68}Ga] Ga-PSMA - 11 Radiopharmaceutical

- The radiochemical purity of $^{68}GaCl_3$ was ≥ 99.9% (TLC & HPLC method) (Fig. 24 and Fig. 25).
- The residual solvent DIPE in $^{68}GaCl_3$ was within the specified value (GC method) (Fig. 26).
- The radionuclidic purity of ^{68}Ga was > 98% (determined by HPGe) (Fig. 27).
- The radiochemical purity of ^{68}Ga-PSMA-11 was ≥ 95% (TLC, PC & HPLC method) (Fig. 28, Fig. 29 and Fig. 30).
- The metal content of $^{68}GaCl_3$ (Fe, Cu and Zn) were within the specified values.
- The Bacterial endotoxin in $^{68}GaCl_3$ and ^{68}Ga-PSMA-11 was < 5 EU/mL (PTS method).
- Each batch were evaluated for sterility test and each batch passed the sterility test.
- A typical PET-CT scan of ^{68}Ga-PSMA-11 of a patient diagnosed with prostate carcinoma is given below (Fig. 31).

Physicochemical and Biological Quality Control Results of $^{68}GaCl_3$ are shown in Table 3.

Table 3. Physicochemical and Biological Quality Control Tests Of $^{68}GaCl_3$

Batch no.	Appearance	pH	Half-life (min)	RC Purity (%)	RN Purity ^{68}Ga (^{67}Ga) (%)	Fe µg/ml	Cu µg/ml	Zn µg/ml	BET test (<3 EU/ml)	Sterility test
1	Clear solution	< 2	69	100	99.95 (0.05)	< 3	BDL	BDL	Passed	Passed
2	Clear solution	< 2	69	100	99.89 (0.11)	< 3	BDL	BDL	Passed	Passed
3	Clear solution	< 2	69	100	99.85 (0.15)	< 3	BDL	BDL	Passed	Passed
4	Clear solution	< 2	69	100	99.97 (0.03)	< 3	BDL	BDL	Passed	Passed
5	Clear solution	< 2	69	100	99.81 (0.19)	< 3	BDL	BDL	Passed	Passed
6	Clear solution	< 2	69	100	99.83 (0.17)	< 3	BDL	BDL	Passed	Passed

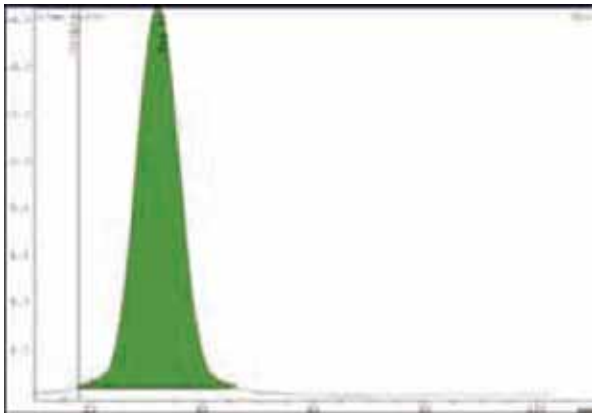

Fig. 24: TLC Spectra of $^{68}GaCl_3$

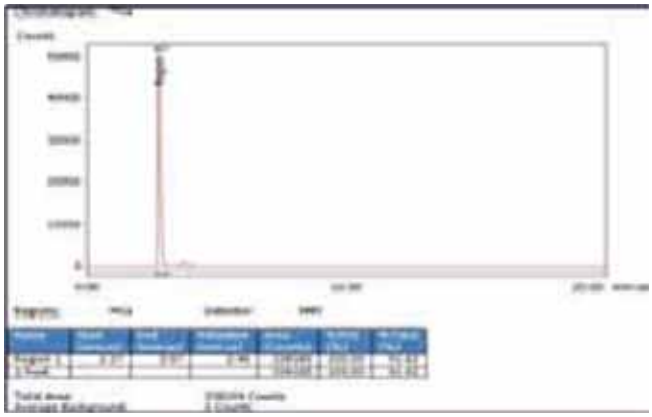

Fig.25: HPLC Spectra of $^{68}GaCl_3$

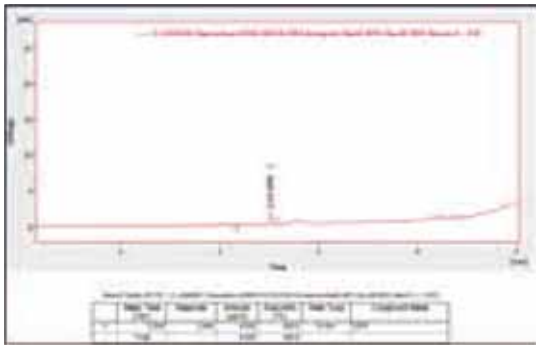

Fig. 26: GC Spectra of $^{68}GaCl_3$

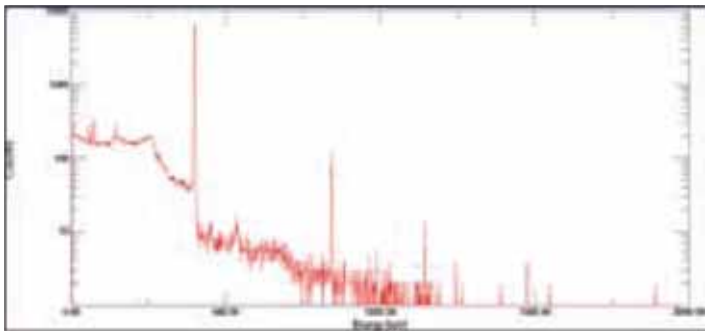

Fig. 27: HPGeSpectra of $^{68}GaCl_3$

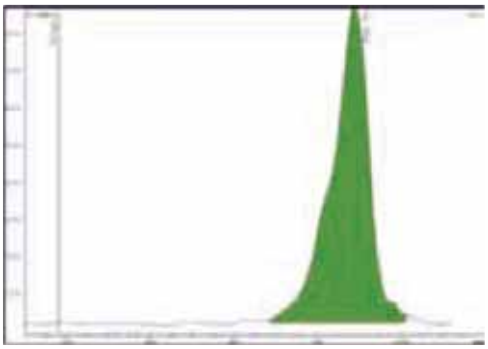

Fig. 28: TLC Spectra of [^{68}Ga]Ga-PSMA-11

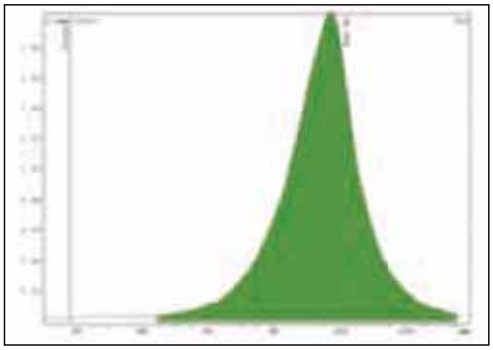

Fig. 29: PC Spectra of [^{68}Ga]Ga-PSMA-11

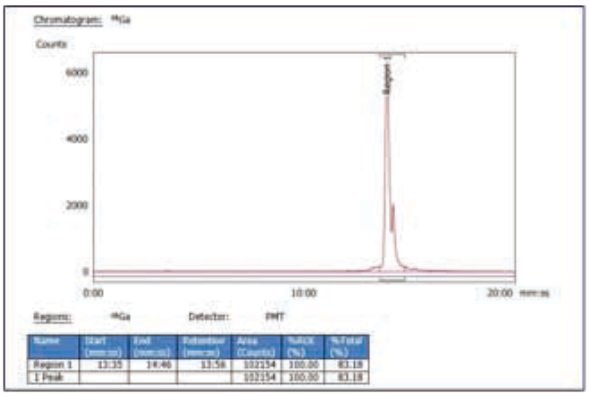

Fig. 30: HPLC Spectra of [^{68}Ga]Ga-PSMA-11

Fig. 31: PET-CT Image of [^{68}Ga]Ga-PSMA-11

Acknowledgements

The authors acknowledge Director VECC, Dr. Sumit Som, for his support and Nuclear Medicine Centres in Kolkata, for participation in clinical studies. The authors also acknowledge colleagues of RC, BRIT Kolkata, and colleagues of MCF, VECC, for their contribution to this work.

References

1. Meyer, G.J., Matzke, K.H., Hamacher, K., Fuchtner, F., Steinbach, J., Notohamiprodjo, G., Zljlstra, S. 'The stability of 2-[F]fluoro-deoxy-D-glucose towards epimerisation under alkaline conditions. Applied Radiation and Isotopes 51/1**(1999)** 37-41.

2. Rijin, C.J.S.V., Herscheid, J.C.M., Visser. G.W.M., Hoekstra. A. 'On the stereoselectivity of the reaction of [^{18}F]acetylhypo□uoride with glucals.' International Journal of Applied Radiation and Isotope. 36 **(1984)**111–115.

3. Lebowitz, E., Greene, M. W., Fairchild, R., Bradley-Moore, P. R., Atkins, H. L., Ansari, A. N., Richards, P., Belgrave, E. 'Thallium-201 for medical use'. Int. Journal of Nuclear Medicine 16/2**(1975)** 151-155.

4. Schwaiger, M., Melin, J. 'Cardiological applications of nuclear medicine'. The LANCET 354 **(1999)** 661-666.

5. Mikolajczak, R., Garnuszek, P. 'Radiopharmaceuticals in cardiology'. Nuclear Medicine Review. 15/1 **(2012)** 39–45.

6. Qaim, S. M., Weinreich. R., Ollig. H. 'Production of ^{201}T1 and ^{203}Pb via proton induced nuclear reactions on natural thallium'. Int. Journal of Applied Radiation and Isotope30/2 **(1979)** 85-95.

7. USP Monographs: Thallous Chloride Tl-201 Injection. USP29-NF24 **(2008)** Page 2108.

8. Cyclotron Produced Radionuclides: Physical Characteristics and Production Methods. IAEA-TRS-468. IAEA, Vienna, **(2009)**.

9. Velikyan, I.,'^{68}Ga-based radio-pharmaceuticals: production and application relationship'. Molecules 20 **(2015)** 12913–12943.

10. Rahbar, K., et al, 'German multicentre

study investigating ^{177}Lu-PSMA-617 radioligand therapy in advanced prostate cancer patients. Journal of Nuclear Medicine 58 **(2017)** 85–90.

11. Amor-Coarasa, A., Schoendorf, M., Meckel, M., Vallabhajosula, S., Babich, J.W. 'Comprehensive quality control of the ITG ^{68}Ge/^{68}Ga generator and synthesis of ^{68}Ga-DOTATOC and ^{68}Ga-PSMA-HBED-CC for clinical imaging'. J. Nucl. Med. 57**(2012)** 1402–1405.

12. Banerjee, S.R., Pomper, M.G. 'Clinical applications of gallium-68'. Applied Radiation and Isotopes 76 **(2013)** 2–13.

13. Oberg, K. 'Gallium-68 somatostatin receptor PET/CT: is it time to replace ^{111}Indium-DTPA octreotide for patients with neuroendocrine tumors? Endocrine 42 **(2012)** 3–4.

14. Schwenck, J., Rempp, H., Reischl, G., Kruck, S., Stenzl, A., Nikolaou, K., Pfannenberg, C., FougereL.A, C.'Comparison of ^{68}Ga-labelled PSMA-11 and ^{11}C-choline in the detection of prostate cancer metastases by PET/CT'. Eur. J. Nucl. Med. Mol. Imaging 44 **(2017)** 92–101.

15. Tirosh, A., Kebebew, E. 'The utility of ^{68}Ga-DOTATATE positron-emission tomography/computed tomography in the diagnosis, management, follow-up and prognosis of neuroendocrine tumors'. Future Oncol. 14 **(2018)** 111–122.

16. Alves, F., Alves, V.H., Neves, A.C.B., Do Carmo, S.J.C., Nactergal, B., Hellas, V., Kral, E. Gonçalves-Gameiro, C., Abrunhosa, A.J., 'Cyclotron production of Ga-68 for human use from liquid targets: from theory to practice'. AIP Conf. Proc. **(2017)** 1845 020001 https://doi.org/10.1063/1.4983532.

17. Blaser, J.P., Boehm, F., Marmier, P., Peaslee, D.C., 'Fonctionsd'excitation de la reaction (p, n). (I)'. Helv. Phys. Acta 24 **(1951)** 3–38.

18. Howe, H.A. '(p, n) cross sections of copper and zinc'. Physical. Review. 109**(1958)** 6–8.

19. Szelecsenyi, F., Boothe, T.E., Takacs, S., Tarkanyi, F., Tavano, E. 'Evaluated cross section and thick target yield data bases of Zn + p processes for practical applications'. Applied Radiation and Isotope 49, **(1998)** 1005–1032.

20. International Atomic Energy Agency. Gallium-68 Cyclotron Production. IAEA-TECDOC-1863. IAEA, Vienna, **(2019).**

21. Sadeghi, M., Kakavand, T., Rajabifar, S., Mokhtari, L., Rahimi-Nezhad, A. 'Cyclotron production of ^{68}Ga via proton-induced reaction on ^{68}Zn target'.Nukleonika 54 **(2009)** 25.

22. Bois, F., Noirot, C., Dietemann, S., Mainta, I. C., Zilli, T., Garibotto, V., Walter, M. A. '[^{68}Ga]Ga-PSMA-11 in prostate cancer : a comprehensive review'. Am. J.Nucl. Med. Mol. Imaging 10/6**(2020)** 349-374.

Performance of MTP-1200 Transportation Cask under 9m Drop Test

*Mukhar Sharma, Dhiren Sahoo, *Pradip Mukherjee*

Radiation Technology Development (RTD); *Chief Executive, BRIT

(Corresponding author: mukhar.sharma@britatom.gov.in)

Abstract

Board of Radiation and Isotope Technology has developed MTP-1200 transportation cask which is designed to carry 44.4 TBq (1200 Ci) of ^{99}Mo radioisotope. The cask uses tungsten heavy alloy as primary shielding material which makes it compact and light in weight. The cask is designed as a leak tight container to carry ^{99}Mo radioisotope in liquid solution form. The package confirms to all the requirement for normal conditions & accidental conditions of transport and qualified as a Type B(U) as per International Atomic Energy Association (IAEA) SSR-6 and Atomic Energy Regulatory Board (AERB) NFR-TS/SC-1.

The critical qualifying requirement among the many others is that the package should maintain its structural integrity under 9m drop test on an unyielding target, depicting the accidental condition of transport. Numerical simulation with explicit finite element method using PAM-Crash code is carried out to study the performance of the package under the 9m drop test in different possible drop orientation. This paper brings out the analysis methodology & performance evaluation of the MTP-1200 cask under 9m drop test. The observed deformation, stresses, g-loading, bolt-stresses etc. in the numerical simulation are discussed.

Keyword: Type B(U), cask, tungsten, structural integrity

Introduction

The transportation of radioactive material is highly regulated & continuously monitored by the concerned regulating authorities. About 20 million consignments of radioactive material transported across the worldwide in a year [1]. Every year a large quantity of Molybdenum-99 (^{99}Mo) is transported for the purpose of radiopharmaceuticals. The decay product of ^{99}Mo, i.e. Technetium-99m (^{99m}Tc), is the workhorse isotope in nuclear medicine for diagnostic imaging and is used in about more than half of all diagnostic/therapeutic application of radiopharmaceuticals. It is used in hospitals, radiopharmacies, laboratories etc. for different applications like detection of disease, study of organ structure & its functions etc.

^{99}Mo has a short half-life of 66 hours only, thus it cannot be stockpiled for use [2][3]. It must be produced & transported on regular basis to ensure continuous availability. BRIT is also now coming up with a new ^{99}Mo production facility "Fission Molybdenum Plant". The ^{99}Mo produced from the said facility will be transported across the world. This necessitates for the development of a high

capacity transportation cask for ^{99}Mo radioactive isotope.

Board of Radiation & Isotope Technology (BRIT) has designed an MTP-1200; ^{99}Mo radioisotope transportation cask. It has been designed for a maximum capacity of 44.4 TBq (1200 Ci) of ^{99}Mo radioisotope. This cask uses tungsten heavy alloy as primary shielding material to make it compact and light in weight. The fabrication of the one-of-a-kind tungsten block in such big size & shape was a major challenge in the process of development. The powder metallurgy process is used to fabricate the tungsten blocks. The critical parameters in the powder metallurgical process like sintering temperature, time-duration of sintering, heating & cooling rate etc. were determined & validated through a series of experiments (not in the scope of paper). The explode view of the MTP-1200 cask is given in Fig. 1

The MTP-1200 transportation cask consists of the cask (^{99}Mo container), carrying the radioactive material and the outer enclosure, used during the safe transportation of the cask. The cask consists of an outer shell, inner shell, tungsten shielding, shield plug, top cover plate and ^{99}Mo housing. Tungsten shielding blocks is encased in type 304 (L) stainless steel shell (i.e. inner & outer shell) providing the necessary structural integrity to the cask under any internal or external loads during its service life. Shield plug, which consists of tungsten shielding block encased in type 304 (L) stainless steel shell, is placed over the cask body. Shield plug is retained over the cask with the help of a top cover plate which is duly fastened with the cask lower part using 6 nos. of M10 bolts. Three number of O-rings are provided at three locations to ensure the leak tightness in the cask. The cask is transported inside an outer enclosure made of type 304 (L) stainless

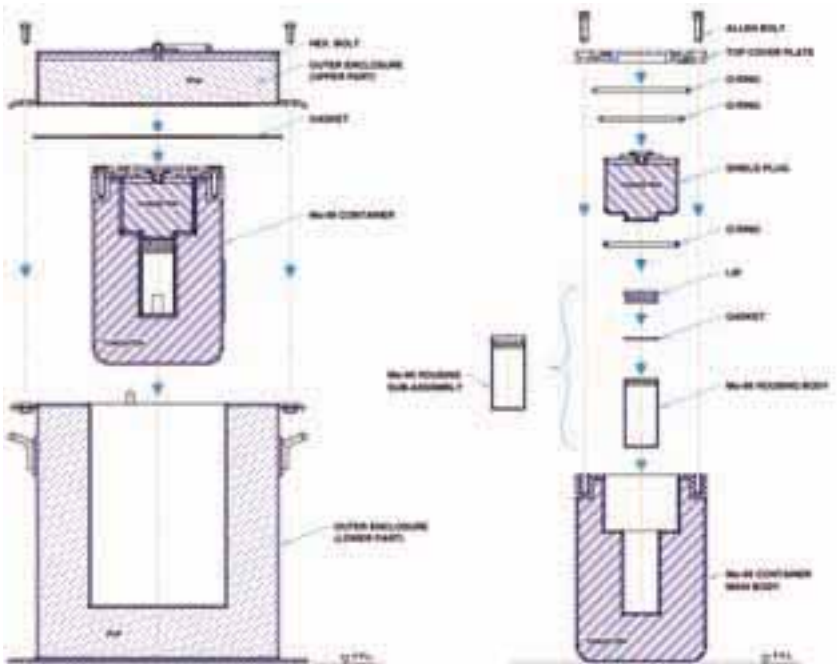

Fig. 1: Exploded view of MTP-1200 cask

steel and filled with poly-urethane foam which act as an impact limiter and fire retardant.

The transportation cask has been designed as a Type B(U) package which needs to qualify normal as well as accidental condition of transport as per the national & international standards [4] [5] [6]. As per these regulations, the transportation cask is required to maintain its structural as well as shielding integrity when dropped on an un-yielding target under the 9m drop test. Various drop orientations such as vertical drop, inverted corner crop, horizontal drop,is considered for the analysis. The paper discusses the structural performance of the MTP-1200 cask under various drop orientation.

Numerical Simulation

Numerical simulation using explicit finite element method is carried out to analyze structural performance of the package. The "PAM-Crash" solver [7] is used to analyze the drop/impact problem. In finite element method, the applicable governing equation of motion in matrix form of a discretized body is given by,

$$[M]\{\ddot{x}\} + [K]\{\dot{x}\} = F_{ext}$$

Where [M] is mass matrix, [K] is stiffness matrix, F_{ext} is external nodal force and $\{\ddot{x}\}\&\{\dot{x}\}$ are acceleration and displacement nodal vector respectively. The drop test analysis is nonlinear in nature & is time dependent. The explicit analysis is mostly used to solve the time dependent non-linear problems. The time dependent field variables in explicit analysis are calculated at nodal points using central difference time integration techniques. Time step in explicit analysis is the critical parameter and the convergence of solution depends upon time step. The upper limit of critical time is given by,

$$\Delta t \leq \frac{h_{min}}{c} \quad where \; c = \sqrt{\frac{E}{\rho}}$$

Where h_{min} is the length of smallest element, c is the velocity of stress wave which depends upon material properties, elastic modulus (E) and density (p).

Model Description

Fig. 2 (a) & 2 (b) shows the sectional view of the solid model and finite element model of the MTP-1200 cask respectively. The finite element model of the MTP-1200 cask was prepared using Visual Environment tool. The entire structure of the package is discretized using 3D shell, tetrahedral, brick and beam elements. All the plate structures are modeled using 3D, 4 node bilinear, Belytchko-Tsay shell elements. Each element is having 6 degree of freedom per node hence, they automatically take into account the rotations i.e. twisting and buckling of plates, direct & bending stresses, which are more predominant in case of impact. One-dimensional beam elements are used to model the bolts. The solid components such as tungsten poly-urethane foam etc. are modelled using 8 node brick elements. The node to node connectivity within components which are physically joined in actual package has been maintained throughout the model. The finite element model consists of 65000 nodes, 40000 solid elements, 14000 shell elements & 66 beam elements.

Fig. 2(a): Volume-cut view of MTP-1200 cask

Fig. 2(b): Finite element model of MTP-1200 cask

Material Modelling

The 9m drop test is an impact event where very high rate of loading and strain rate are expected. In order to simulate the material behavior under the very high strain rate (in the order of $10^2 \sim 10^4$ s^{-1}) Cowper-Symonds strain rate material model is used in the analysis which is widely used in explicit problems. The Cowper-Symonds model governing equation is given by,

$$\frac{\sigma_d}{\sigma_s} = 1 + \left(\frac{\dot{\varepsilon}}{C}\right)^{\frac{1}{P}}$$

where, σ_d is dynamic yield stress, σ_s is static yield stress, is strain rate, C & P are material constants. The Table-1 shows the mechanical properties of the materials used in the analysis. The properties of the polyurethane foam (PUF) used in the analysis were taken from the quasi-static & dynamic response observed in the experimental compression tests carried out with PUF specimens at different strain rates [8]. Fig.3 shows the Stress-strain curves for polyurethane foam subjected to quasi-static and dynamic compression.

Table 1: Material Property [8], [9], [10]

Sr. No.	Properties	Steel (SS 304L)	Tungsten	PUF	Bolt (12.9 Grade)
1	**Material law**	Bilinear Elastic-Plastic	Bilinear Elastic-Plastic	Bilinear Elastic-Plastic	Linear Elastic
2	**Density**	7800 kg/m³	18100 kg/m	320	7800 kg/m³
3	**Young's modulus**	210 E9 N/m²	4 E11 N/m²	88.91 E6 N/m²	210 E9 N/m²
4	**Poisson's ratio**	0.3	0.28	0.2	0.3
5	**Yield stress**	170 E6 N/m²	651 E6 N/m²	23.76 E6 N/m²	1080 E6 N/m²
6	**Tangent modulus**	787.5 E6 N/m²	4036.31 E6	--	24.705 E9
7	**Ultimate stress**	485 E6 N/m²	787 E6 N/m²	--	1200 E6 N/m²
8	**Shear modulus**	76.9 E9 N/m²	156 E9 N/m²	37.045 E6	--
9	**Bulk modulus**	167 E9 N/m²	303 E9 N/m²	49.394 E6	--

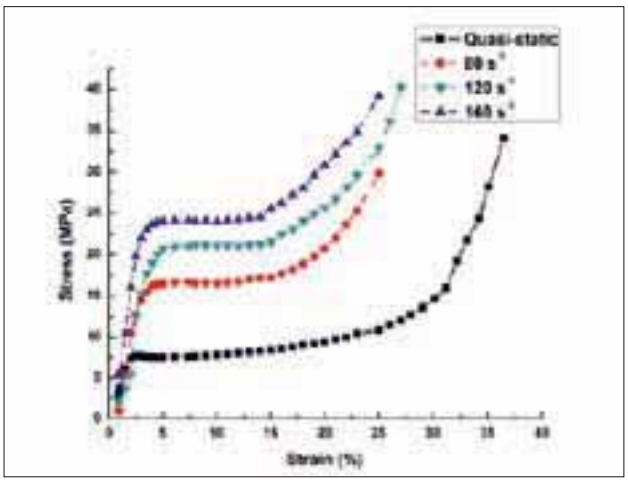

Fig. 3: Stress-strain curves for polyurethane foam subjected to quasi-static and dynamic compression [8]

Loading Conditions

The three potentially most damaging orientations namely vertical drop, horizontal drop, inverted corner drop as shown in Fig. 4 (a), 4 (b), 4 (c) were considered for the 9m drop test on an unyielding target. The target is considered as a planar rigid wall of infinite mass so that all the impact energy is absorbed back by the MTP-1200 cask only imparting maximum possible damage. The MTP-1200 cask is provided with a velocity of 13.36 m/s which is equivalent to the velocity acquired by the package while hitting the target when dropped from a height of 9m. It is ensured in all the drop orientation that the line joining the center of gravity of the package and the point of contact always remain perpendicular to the unyielding target. Self-impacting with edge treatment contact was defined for the drop analysis. Frictionless contact condition was specified between the model and the rigid wall.

Results & Discussion

The structural performance of the MTP-1200 cask under 9m drop test was analyzed for various potentially most damaging drop orientation viz. vertical drop, horizontal drop, inverted corner drop. The structural integrity of the MTP-1200 cask was analyzed using various critical parameters such as von-misses stress, equivalent plastic strain, stress intensity, bolt stress, energy absorbed by various components etc.

Fig. 4(a): Vertical drop of MTP-1200 cask

Fig. 4(b): Horizontal drop of MTP-1200 cask

Fig. 4(c): Inverted corner drop of MTP-1200 cask

Vertical Drop

The sectional view of the MTP-1200 cask after 9m vertical drop test is shown in Fig. 5(a). It can be observed that the poly-urethane foam in the outer enclosure gets deformed and compacted at the bottom after the impact. No significant deformation is observed in the cask or other components. Energy absorbed by the various components is shown in Fig. 5(b). It can be observed from the Fig. 5(b) that the maximum energy has been absorbed by PUF material which justifies its usage as impact limiter. The maximum von-misses stress in the outer shell is 288.30 MPa, as shown in Fig. 5(c), which is well within the ultimate stress of 485 MPa. The outer shell acts as containment boundary which houses the tungsten shielding material in the cask. However, even the localize failure of the outer shell will not lead to the possible shielding loss in the regulatory required 800°C fire test due to the very high melting point temperature of shielding material i.e. tungsten heavy alloy [4].

The tungsten shielding component is critical for the shielding integrity of the cask. The maximum stress intensity in the tungsten shielding material is 376.80 MPa as observed in the Fig. 5(d) whereas the allowable limit of stress intensity is 787 MPa. Thus, the tungsten shielding component maintains its structural as well as shielding integrity in the accidental drop test.

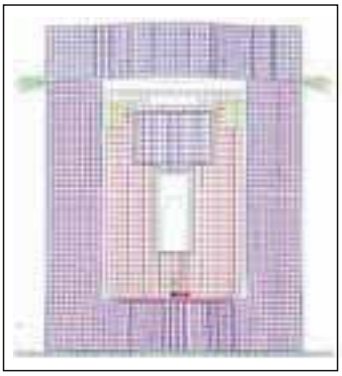

Fig. 5(a): Sectional view of MTP-1200 cask after 9m vertical drop

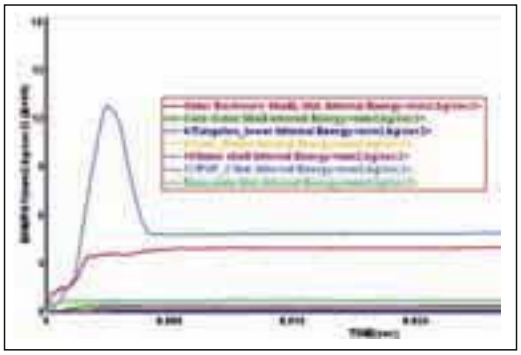

Fig. 5(b): Internal energy absorbed by various components under 9m vertical drop

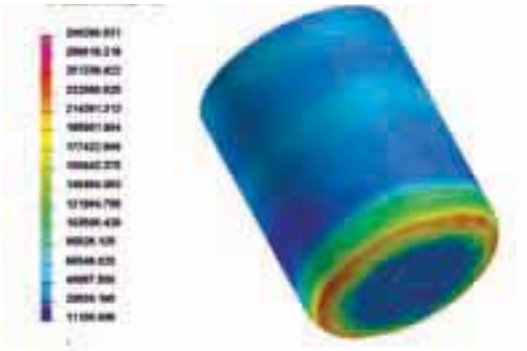

Fig. 5(c): Von-misses stress observed on the outer shell under 9m vertical drop

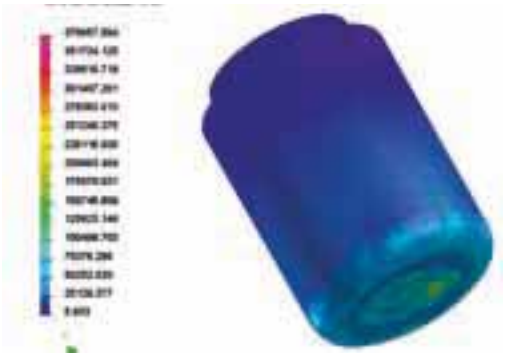

Fig. 5(d): Stress intensity observed on the tungsten part under 9m vertical drop

Horizontal Drop

The analysis of horizontal drop is critical to examine the possible protruding effect of flange attached with the outer enclosure. It is also essential to study the performance of fasteners in the cask & the outer enclosure under shear load. Fig. 6 (a) shows the gross deformation of the package under the horizontal drop test. The deformation in the flange shows that the initial bend provided in the flange allows it to deform on impact instead of protruding inside.

The von-misses stress contour on the outer shell given in Fig. 6(b) shows the effect due to the horizontal drop orientation impact. The observed maximum stress i.e. 313.80 MPa is also within the permissible limit. The maximum equivalent plastic strain in the outer shell is found to be 1.3 %. No considerable deformation is observed in the outer shell. Similarly, the maximum stress intensity observed in the tungsten shielding components i.e. 363.60 MPa [shown in Fig. 6(c)], is also well within the respective ultimate stress. Hence, the MTP-1200 cask is safe under the horizontal drop orientation.

Fig. 6(a): Sectional view of MTP-1200 cask after 9m horizontal drop

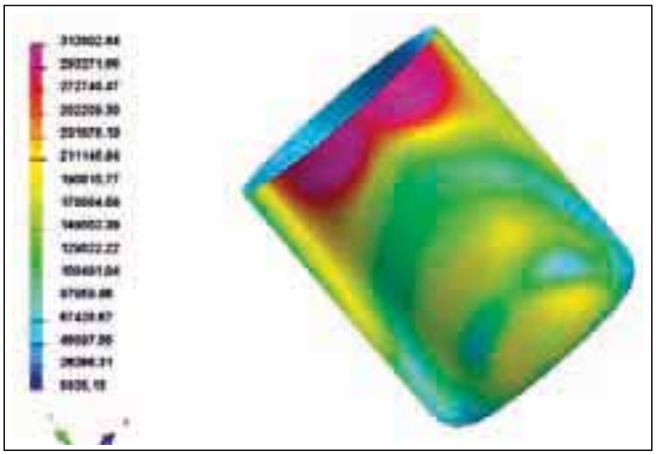

Fig. 6(b): Sectional view of MTP-1200 cask after 9m horizontal drop

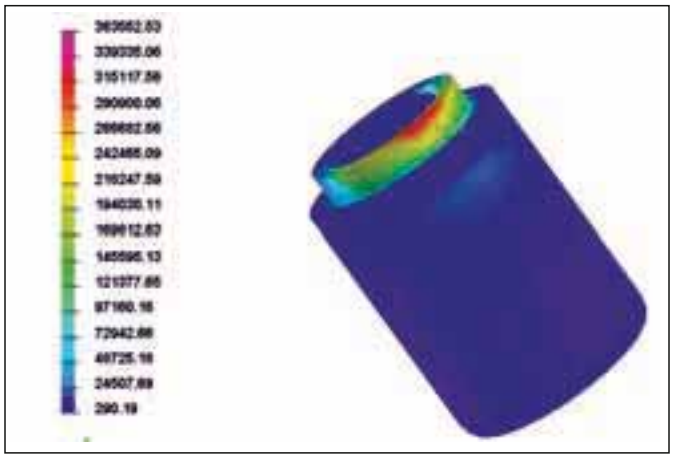

Fig. 6(c): Stress intensity observed on the tungsten component under 9m horizontal drop

Inverted Corner Drop

Fig. 7 (a) shows the gross deformation in the MTP-1200 cask under 9m inverted corner drop test. It can be observed that the upper portion of the outer enclosure grossly deformed in the impact & absorb the maximum internal energy. The energy absorb by various components in the drop is shown in the Fig. 7(b). It can be observed that the maximum amount of the impact energy is absorbed by the Poly-urethane foam material filled in the outer enclosure cavity and acting as an excellent impact limiter. The maximum von-misses stress observed in the outer shell is absorbed in the Fig. 7(c). The outer shell shows a maximum von-misses stress of 298.70 MPa, which is well below the respective ultimate stress i.e. 485 MPa. Fig. 7(d) shows the maximum stress intensity observed in the tungsten component. The observed maximum stress intensity of 470.80 MPa in the tungsten component is also well below the permissible limit i.e. 787 Mpa.

The maximum shear stress observed in the M-10 bolts securing the shield plug with the cask body in the vertical, horizontal and inverted corner drop are 163.40 MPa, 217.34 and 466.24 respectively. The maximum shear stress is expected in the horizontal drop as the bolts are directly subjected to the shear load. However, the maximum shear stress is observed in the inverted corner drop test probably due to their close vicinity with the point of impact & availability of less PUF at the location. Whereas maximum axial stress observed in the M-10 bolts in the vertical, horizontal and

Fig. 7(a): Sectional view of MTP-1200 cask after inverted corner drop

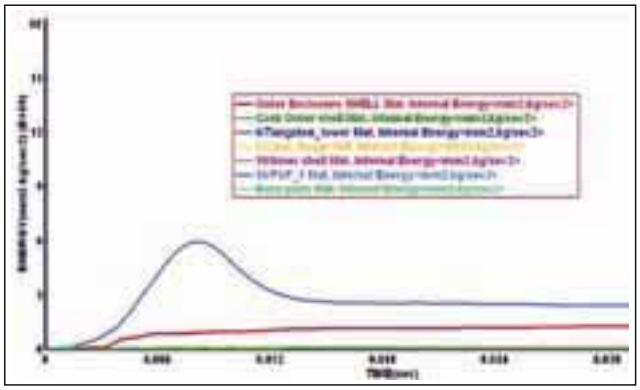

Fig. 7(b): Energy absorbed by various components

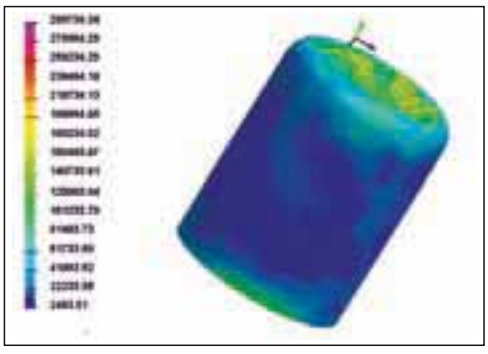

Fig. 7(c): Von-misses stress observed on the outer shell under 9m inverted corner drop

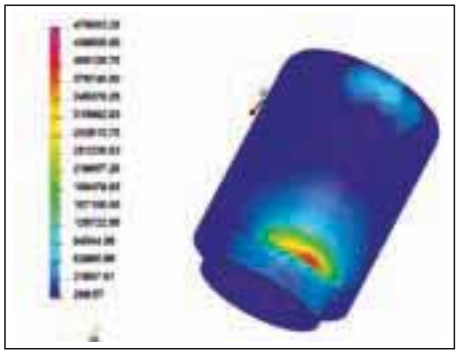

Fig. 7(d): Stress intensity observed on the tungsten part under 9m inverted corner drop

inverted corner drop are 434.75 MPa, 521.31 and 142.20 respectively. The maximum stresses observed in the M-10 bolts are within the allowable limit and meets ASME qualifying criteria Sec. III Appendix F [11]. Hence, all the M-10 bolts are safe under the all the drop orientation.

Conclusion

The MTP-1200 cask was analysed using explicit finite element method to study its performance under 9m drop test as per IAEA and AERB guidelines. The stress intensity of the critical components such as tungsten, outer shell etc. is found to be well within the safe limit and meet the ASME criteria. There is no considerable deformation observed in the outer shell and tungsten. Combined stresses in bolts of the cask are also within the limit and meet the ASME criteria. Hence, the package maintains its structural integrity under 9-meter drop test.

References

1. The Role of Safety and Security in Transport of Radioactive Material Discussed at Vienna Conference; IAEA Office of Public Information and Communication; (2021).

2. Essentials of Nuclear Medicine and Molecular Imaging (Seventh Edition), (2019).

3. Jr.Mettler Fred A., Guiberteau Milton J. (Eds) Radioactivity, Radionuclides, and Radiopharmaceuticals; "Essentials of Nuclear Medicine and Molecular Imaging", (Seventh Edition)(2019), pp 1-18.

4. IAEA Safety Standards "Regulations for the Safe Transport of Radioactive Material", (2018) Edition Safety Requirements No. SSR-6.

5. IAEA (ed.), "Advisory Material for the IAEA regulations for the safe transport of radioactive material" Safety Guide SSG-26, (2012), IAEA, Vienna.

6. AERB (ed.), "Regulation for Safe Transportation of Radioactive Material", AERB/ AERB/NRF-TS/SC-1 (Rev.1), (2015), India.

7. PAM-CRASH Version-6.8, ESI, France.

8. ManeJ.V., Chandra A., Chandra S. "Mechanical property evaluation of poly-urethane foam under quasi-static and dynamic strain rates- An experimental study". Procedia Engineering 173 (2017) 726-731.

9. RohrI., NahmeH., Thomas K., Anderson C.E. "Material characterization and constitutive modelling of a tungsten-sintered alloy for a wide range of strain rates". Internat.J.Impact Engg. 35 (2008) 811-819.

10. ASME, "Boiler and Pressure Vessel Code", Section II, Materials, Part D(2015).

11. ASME, "Boiler and Pressure Vessel Code", Section III, Div. 1 Appendix F: "Rules for Evaluation of Service Loadings with Level D Service Limits", (2015).

Drug-Radiopharmaceutical Interactions and Its Effect on Radiopharmaceutical Pharmacokinetics: A Review

[1,2*]*Ashok R. Chandak,* [2]*B. L. Malpani and* [2]*M. K. Ray*

[1]**Radiopharmaceutcal Laboratory, BRIT;**[2]**Radiation Medicine Centre, BARC**

(Corresponding author:ashok.chandak@britatom.gov.in)

Abstract

Untoward or unexpected pharma cokinetics is one of the most common problems associated with radiopharmaceuticals which can have a significant clinical impact on safety, scan interpretation, imaging accuracy and may contribute unnecessary radiation dose to the patients. Considerable evidence exists in regard to the potential for altered biodistribution of radiopharmaceuticals resulting from the co-administration of therapeutic drugs, as well as, from the suffering of certain disease states, nutritional conditions, and other factors. The present article provides an overall summary of altered pharmacokinetics of radiopharmaceuticals while using different radioisotopes (^{99m}Tc, ^{68}Ga, ^{67}Ga, ^{18}F, ^{201}Tl, ^{131}I and ^{177}Lu) and related products, with a special focus on the factors affecting localization, and also to stimulate the pharmacists who provides clinical pharmacy services to nuclear medicine. Although most drug-radiopharmaceutical interactions are not beneficial, some nuclear medicine procedures are conducted using drug intervention to enhance the diagnostic efficacy of the tests, and, sometimes to reduce the radiation toxicity. This review provides organ-wise summary of various aspects that can indicate possible interactions between drug and radiopharmaceuticals and highlights factors to exemplify the significance of altered pharmacokinetics of radiopharmaceuticals in the tabulated form to allow the easy access of source material.

Introduction

Radiopharmaceuticals are pharmaceutical compounds tagged with suitable radioisotope which is used in oncology for the initial staging, to evaluate response to treatment, residual and recurrence of disease after the treatment, and restaging of the disease among the different types of tumor. These are also used for treatment of various diseases and cancer [1]. Combining drugs with drug or radiopharmaceutical may cause pharmacokinetic and/or pharmacodynamic interactions. Pharmacokinetic mechanisms of interaction include alterations of absorption, distribution, biotransformation, or elimination. Absorption can be altered when drugs that alter pH or motility are co-administered, as seen with certain antiulcer or antidiarrheal medications, or when drugs are chelators or adsorbents [2]. The uptake of ^{99m}Tc-labelled compounds and ^{67}Ga by brain tumors decreases due to reduction in intracellular edema if the patient is taking glucocorticoids. Distribution variations can result from competition for protein binding or displacement from tissue-

binding sites. Induction of gene expression (slow), activation or inhibition of liver and extrahepatic enzymes such as CYP 450, and conjugating enzymes have long found a place of choice in the literature describing the potential for adverse drug interactions resulting from altered metabolism. For example, bone uptake of MIBI increased in hyperparathyroidism which is a series of syndromes that causes calcium and phosphorus metabolism disorder due to excessive secretion of parathyroid hormone [3]. Induction of metabolic activities in the liver is well described with the major anticonvulsant medications phenytoin, carbamazepine, and barbiturates, whereas, inhibition can occur with antimicrobials from the quinolone, macrolide, and azole families. Finally, excretion can also be modified by drugs that change urinary pH, as carbonic anhydrase inhibitors or change secretion and reabsorption pathways by drugs such as probenecid. Pharmacokinetic interactions in general result in an altered concentration of active drug or metabolite in the body. Pharmacodynamic interactions except antagonist effects are uncommon in case of radiopharmaceutical preparations as the active tracer concentration is in the nano molar or pico molar level and which does not produce any pharmacological action on body [4].

Drug interactions and adverse drug effects have received much attention since studies published have shown the upwards trend each year being hospitalized, as well as leading to the death of a number of patients [5]. One principal objective of the drug development process is the generation of scientific information on drug interactions so that treating physicians will have the data necessary to proceed with safe clinical treatment involving more than one medicine [4][5]. Adverse drug reaction is an important cause of drug related problems and this includes significant morbidity and mortality.Drug interactions may occur between prescription drugs, between food & drug and chemical & drug. Combining drugs may cause pharmacokinetic and/or pharmacodynamic interactions [6].

Adverse event reporting database provides no information on incidence, as events may not be recognized, and in many countries, reporting is not mandatory. There are numerous drug radiopharmaceutical interactions that will alter nuclear medicine images and procedures. The incidence of drug-radiopharmaceutical interactions is unknown. According to drugs and cosmetic act and rules, 1945, radiopharmaceuticals have been governed by “Schedule K” [7]. Drugs specified in schedule K shall be exempted from all the provisions of chapter IV of the act made there under to the extent and subject to the conditions of exemptions specified in the schedule (Schedule K, Drugs and Cosmetic Act 1940 and Rules, 1945). First time Indian Pharmacopoeia (IP) - 2014 and addendum 2015 have incorporated 28 radiopharmaceutical monographs in the official format provided by BRIT/BARC, Department of Atomic Energy (IP 2014) which is very early placed in USP/BP (USP 1955) [8]. In India there is no reported case of adverse reaction, except the poor imaging or false (positive or negative) imaging of target organ, many suspected interactions may eventually be proven false due to chance or non-causal associations. One survey in

Japan reported a rate of more than 1 event per 100,000 administrations [9]. One European study on adverse reaction with radiopharmaceuticals, conducted in late nineties, reported a rate of 11 (4-19) events per 100,000 administrations [10][11]. These relatively low rates of adverse events may be explained, at least partially, by the usually small mass of drug administered. Additionally, radiopharmaceuticals are typically administered only once or at very limited number of times to any given patient limiting the potential for allergic reactions and events which might be caused by cumulative exposures [12]. Small number of reported cases, studies has demonstrated that less than 10% of possible adverse reactions are actually reported [13].

Radiopharmaceuticals are administered in the form of a traced compound to a patient in order to examine abnormal distribution or physiological malfunctioning in the body. There is a considerable indication that biodistribution and pharmacokinetics of radiopharmaceuticals may be altered by a variety of drugs, food, disease conditions and surgical procedures [14]. Sometime the unknown and unrecognized interactions of radiopharmaceuticals with other compounds (food or drug) can lead to a state of total confusion [15]. For example, interactions that result in poor organ visualization may require repeating the procedure, thus resulting in excess irradiation of organs or if the interaction is unrecognized, it may result in misdiagnosis. Such misdiagnosis could delay appropriate treatment (e.g. an interaction that creates false positive or negative findings) and extra dose to patients. The aspects of potential interactions are being studied in-vitro not only with the aim of providing simple understanding but also the findings can be used to predict quantitative events in-vivo, and thereby, avoid or limit undesired clinical interactions.

Sometime due to the miscalibration of equipment for measuring the radioactive dose may cause severe damage to the individual [16]. Any incidence of adverse events associated with radiopharmaceuticals is unknown, at the same time incidence of interactions between radiopharmaceuticals and prescription drugs has not been reported. Drug or chemical agent which alters the chemical identity of the tracer or alters the physiological status of the organ of interest could be expected [17]. The level of prescription drug use and polypharmacy practices, the potential burden of drug-radiopharmaceutical interactions may be significant. The paper reviews the effect of various drugs on the diagnostic and therapeutic radiopharmaceuticals as a helpful guide in practice, but in no way covers all the drug radiopharmaceuticals interactions that may occur. Suspected alterations in biodistribution should be investigated. Care must be taken to ensure that such drugs are discontinued for an adequate time prior to imaging.

The objective of this article is to provide a review for the practitioners of the disciplines embodied in them yet still provide easily obtainable information to non-practitioners about possible interaction in between drug and radio-pharmaceuticals. Various factors that can affect biodistribution of radiopharma-ceuticals with administration of prescribed drugs, miscalibration of equipment and improper labeling of radiopharmaceuticals are the most commonly reported factor [18]. Drug-radiopharmaceutical interactions may

arise as a result of a variety of factors including the pharmacological action of the drug, physicochemical interactions between drugs and radiotracers, and food habits. While we focus on drug-radiopharmaceutical interactions, it is also important to consider that handling and processing may also cause or increase the risk of adverse reactions. For example, contamination during the administration may alter the subsequent biodistribution of the radiopharmaceuticals.

The well-known examples are interactions with the antiseptic's povidone iodine and chlorhexidine. In presence of iodine-based antisepsis, labeled ^{99m}Tc- radiopharmaceuticals, may release free pertechnetate [19][20]. Similarly, chlorhexidine gluconate can react to form technetium gluconate complex, which is taken up by the kidney [15]. Although less commonly reported, radiopharmaceuticals may also interact with the syringe or catheter components [21][22]. Radiopharmaceuticals also have the potential of interaction with cigarette smoking, alcohol intake, and dietary habits (e.g. high dose of vitamins). The concentration of ^{99m}Tc-RBC and ^{99m}Tc-plasma protein in blood decreased among cigarette smokers which affect the performance of nuclear imaging procedures [23]. In recent years the pressure on nuclear medicine to relinquish morphological imaging to better techniques has fueled attempts to develop functional imaging. Radiopharmaceuticals are not only used in cancer patients but also to diagnose the improper functioning of different organs, viz. kidney, heart, brain, hepatobiliary system.

Adverse Drug Reactions (ADR) is generally serious clinical events that may be related to patient characteristics, environment, and the particular exposure. However, an ADR is not always a readily detectable clinical event, but instead can be clinically silent [24]. Factors affecting the biodistribution of radiopharmaceuticals can be classified into 5 major categories include (1) radiopharmaceutical preparation and formulation problems; (2) radiopharmaceutical administration techniques and procedures; (3) changes in biochemical and pathophysiology; (4) previous medical procedures such as surgery, radiation therapy and dialysis; and (5) drug interactions [25][26][27]. In the present article the possibility of clinically silent adverse events with radio-pharmaceuticals-drug interactions are considered. This paper reviews the literature on reports of both evidences based and clinically silent adverse reactions associated with radio-pharmaceutical-drug interactions by different organs.

Brain Imaging Agent

The major risk of drug-radiopharmaceutical interactions occurs with pharmaceuticals that can alter the permeability of the blood-brain barrier (BBB) some pharmaceuticals may influence the receptor-bound neurotransmitters [28]. Sodium pertechnetate ($Na^{99m}TcO_4$) widely utilized for scintigraphy studies mainly for thyroid, brain and stomach. If ^{99m}Tc sodium pertechnetate is administered along with aluminum containing antacids or sulfonamides for brain scintigraphy it will fail to leave vascular space may be due to increased blood pool activity. This may cause false results and subsequently, misdiagnosis. Also, cytotoxic drugs such as cyclophosphamide, vincristine, bleomycin and cisplatin are reported to

affect the pharmacokinetic response of tumor-seeking radiopharmaceutical ^{67}Ga-citrate. This radiopharmaceutical localizes in neoplasms as well as liver and regions of infection or inflammation. That may result in a very high uptake of tracer in blood with little or no uptake by the tumor [17][29]. Cerebral retention of ^{99m}Tc-ECD is improved in rats by the administration of probenecid, presumably by saturating the carboxylate transport system [30]. ^{67}Gallium used with other cytostatic drugs except for methotrexate might be used consecutively or together in cancer therapy because it potentiated the cytostatic effect [31].

Suppression of ^{67}Ga-citrate uptake in cerebral tumors among patients taking steroidal preparations (cortisone) which results from a decrease in extracellular sodium and fluid volume [17][32]. As the tracer is often associated with the oedematous fluid, it creates the appearance of a tumor decreased in size in the scintigraph, causing the tumor to be missed completely resulting in misdiagnosis. Patients treated with chelating agent deferoxamine used to treat iron overload and aluminum toxicity there was diffuse tracer activity and poor tissue localization with complete absence of normal uptake by ^{67}Ga-citrate. This occurs because deferoxamine forms a complex with ^{67}Ga, stronger than that of ^{67}Ga with transferrin, thus interfering with ^{67}Ga-transferin binding and subsequent cellular uptake [14][17][32].

The uptake and secretion of ^{99m}Tc-pertechnetate by the gastric mucosa may be affected by drugs, thereby interfering with the imaging of Meckel's diverticulum [14]. Extracts of Ginkgo biloba decreased the uptake of ^{99m}Tc-sodium pertechnetate in the duodenum, kidney and liver [33]. One recent study in the rat brain based on administration of diazepam with ^{18}F-FDG, which shows a progressive decrease of the FDG global uptake, but it does not change local patterns within the brain [34].

Adrenal Gland Imaging Agent

Difference in physiology of adrenal cortex and adrenal medulla regions of the adrenal gland, it is not surprising that these interactions occur with different groups of drugs [35]. Such interactions can have varying effects on the resulting image, depending on whether the drug increases or decreases the uptake of the radiopharmaceutical. In many cases the effect may be predicted based on the known pharmacological actions of the interacting drug [14].

Uptake of ^{131}Iodomethyl-nor-cholesterolaffects in presence of spironolactone secreted by the adrenal cortex. It has been reported to both increase uptake [36][37][38][39], as well as decrease uptake [37][40]. An increase in ^{131}I-Iodomethyl-nor-cholesterol uptake by the adrenal gland is a result of the steroid synthesis from plasma. As such, it may result in false positive diagnosis of adrenocortical adenomas, adrenal incidentalomas and pheochromocytoma [36][37][41][42]. Spironolactone can also decrease aldosterone synthesis by decreasing the uptake of radiolabeled cholesterol by the adrenal cortex. This also has the potential to interfere in tumor diagnosis [14][37].

Oral contraceptives have been found to increase the binding of ^{131}I-Iodomethyl-

nor-cholesterol by increasing plasma renin activity. This results in adrenocortical stimulation and may cause false positives results which complicating the interpretation of adrenal scintigrams potentially requiring retesting and exposing the patient to extra radiation [40][43].

Bone Imaging Agent

The constant remodeling of bone guides the choice of tracers, to identify abnormalities in the bone structure or pathologies related to the remodeling process. Therefore, pharmaceuticals that have an impact in any of these processes have the potential to interact with radio imaging of bone. Due to the complex process involving the uptake of phosphonate by the bone, a number of pharmaceuticals may modify the biodistribution of the ^{99m}Tc-labeled-diphosphonate. For example, etidronate and pamidronate, which are diphosphonates used in the treatment of Paget's disease, compete with MDP (^{99m}Tc-methylene diphosphonate) due to structural similarity may result in false negative images (faulty diagnosis) [44][45]. Administration of estrogen with ^{99m}Tc-MDP accumulates activity in breast tissue. The biodistribution of ^{99m}Tc-PYP (sodium pyrophosphate) may be altered by concomitant use of sodium diatrizoate. Use of diatrizoate with ^{99m}Tc-PYP has been shown to cause significant renal and liver uptake of the radiopharmaceutical, interfering with the performance of nuclear imaging procedures [46]. Diffuse uptake of ^{99m}Tc-PYP used for bone scintigraphy in myocardium when administered along with doxorubicin. In the worst case, this can result in a faulty diagnosis. There have been an extraosseous accumulation of ^{99m}Tc-MDP

Table 1: Drug interaction with phosphonate and its outcomes

Interfering Drug	Effect on Image
Iron containing compounds; Phospho-Soda	Decreased osseous uptake of bone imaging agents, and increased intravascular activity
Iron containing compounds; Amphotericin B; Gentamicin; Cyclophosphamide; Vincristine; Doxorubicin	Increased renal retention
Cytotoxic cancer chemotherapy	Diffuse activity around the calvarium, termed "Sickle Sign"
Aluminum Containing Antacids	Appearance of liver
Sodium diatriazole	Marked renal and hepatic localization of RP
Regional chemoperfusion; Injection of Calcium	
Gluconate, Iron Dextran, Heparin Calcium,	Extraosseous accumulation of RP
Estrogens	Accumulation of RP in breast tissue
Doxorubicin	Diffuse uptake of RP in myocardium

when administer with intramuscular iron dextran, calcium gluconate, heparin calcium injection. Concomitant use of iron dextran modifies the biodistribution of ^{99m}Tc-MDP at the site of injection instead of diffusing throughout the skeleton [47][48]. Localized complexing occurs between reduced technetium and ferric hydroxide which is released from the iron dextran complex. This may prevent or delay the skeletal scintigraphy of tumors [17][49].

Heart Imaging Agent

The most commonly used radio-pharmaceutical for visualizing the heart is cyclotron produced thallous chloride (^{201}Tl) and MIBI labeled with ^{99m}Tc. The use of thallous with atenolol, propranolol (β-blockers) can result in a temporary decrease in the severity of perfusion defects [50]. Beta Blockers will prevent treadmill stress patients from reaching their target heart rate. Discontinued 48 hours before testing is suggested or switch to pharmacologic stress. While β-blockers may interfere in the imaging results, suspending use prior to imaging is not recommended, as it may increase the risk of myocardial ischemia [51]. Other studies have suggested that there is actually a net increase in the assessed severity among patients with minor coronary disease upon angiography [14]. ^{201}Tl uptake was significantly higher in the hearts of doxorubicin treated rats compared to the control rats, indicating a slow wash-out of ^{201}Tl from the myocardium [52][53]. Decrease in severity of perfusion defects upon radio imaging using ^{201}Tl is dependent on the dose of the radiopharmaceutical that goes to heart and the quality of the imaging is insufficient for accurate analysis and in consequence, is of limited value for diagnosis [54]. The radiopharmaceutical ^{99m}Tc-pyrophosphate is widely used to detect myocardial infarctions. Diminished cardiac activity and increased renal activity has been observed with the use of heparinised catheters for *in-vivo* red cell labeling with ^{99m}Tc-pyrophosphate [18][29][55][56]. Xanthines will block the vasodilatory effects of adenosine. Patients should be withheld from caffeine for 6 hours. Patients should withhold theophylline medications for 48 hours prior to a dipyridamole or adenosine study. However, with asthma patients may use dobutamine [57].

Antimyosin labeled with ^{111}Indium is specific for myocyte necrosis and is used in the detection of infarct, myocarditis and cardiac rejection. Chemotherapeutic drugs, notably doxorubicin, have been shown to cause increased myocardial uptake of the radiopharmaceutical [58]. Doxorubicin decreased the uptake of 111-Indium antimyosin by the myocardial cell [59]. One trial investigated effect of dexrazoxane to improve doxorubicin and epirubicin induced cardiotoxicity using 111-Indium antimyosin [60]. Radio-immunoscintigraphy was very sensitive in detecting anthracycline cardiac damage, but its specificity is low and it cannot be considered a primary test for guiding anthracycline treatment. This suggests that ^{111}Indium-antimyosin could potentially be used to monitor the degree of cardiotoxicity produced by doxorubicin and epirubicine [61]. Medication anthracycline antineoplastics, e.g. doxorubicin and epirubucine can affect labelling of RBCs. Drugs may interfere with stannous ions so that stannous is not taken up by the cells, may affect the RBC membrane or may affect the target of

binding by reducing the hematocrit and/or hemoglobin concentration [62].

The extract of Uncaria tomentosa can reduce the uptake of sodium pertechnetate-MIBI and tetrofosmin in heart and may decrease the visualization of the organ, there is potential for misdiagnosis and requiring a repeat procedure [63][64][65]. In delayed myocardial imaging MIBI shows uptake in gut and interferes in the heart imaging which can be corrected by administering lemon and sodium bicarbonate to the patients. Soda lime solution stimulates the gut movement and heart gets differentiated from gut wall and clear heart images can acquire. It is found that cardiac ^{18}F-FDG uptake was significantly lower among diabetics and also among patients taking either benzfibrate or levothyroxine. Cardiac ^{18}F-FDG uptake was significantly higher in men, patients less than 30 years old, patients with heart failure, and those receiving benzodiazepines. Potentially, pharmaceutical manipulation of ^{18}F-FDG may provide an opportunity to optimize PET/CT imaging [66].

Kidney Imaging Agent

Most drugs are metabolized and excreted through the kidney and there is great potential for drug-radio-pharmaceutical interactions. Many drugs alter kidney function in a dose dependent manner. Appropriate imaging in uro-oncology is a crucial component at primary diagnosis, follow up and recurrence to achieve accurate assessment of the disease and determine the most effective treatment. The literature on positron emission tomography in uro-oncology has shown a great number of radio-pharmaceuticals that may be used for urological malignancies for prostate cancer e.g. ^{18}F-fluorodeoxyglucose, ^{11}C-choline, ^{18}F-fluorocholine, ^{11}C-acetate and ^{18}F-fluoride [67].

In patients with unilateral renal artery stenosis, angiotensin converting enzyme inhibitors (ACE-Inhibitors) decrease glomerular filtration in the affected kidney by the interruption of autoregulatory mechanism causing problems in the distribution of the radiopharmaceuticals [14]. A case report showed that calcium antagonists can cause false-positive captopril renograms (Table 2). These medications should be stopped before captopril renography, and physicians should be aware of this possible drug interaction if bilateral symmetrical renal function deterioration is seen in a patient's captopril renogram [68].

The use of drugs like dipyridamole increases or depending on the concentration may decrease the excretion of ^{99m}Tc-DTPA by the kidney [69]. Diuretics as furosemide may improve renal function so that misleading good renograms and flow curves are obtained when using the renal imaging agent ^{99m}Tc-DTPA [17].

Gomes et al. noted that mitomycin-C increased the uptake of ^{99m}Tc-DTPA by the spleen and liver and also increased the uptake of ^{99m}Tc-GHA by the liver causing misdiagnosis and or a false positive result [70]. ^{99m}Tc-glucoheptate (GHA) is widely used to visualize renal structures (static imaging), particularly kidney parenchyma. Concurrent administration with penicilamine, penicillin-G potassium, penicillin-V potassium, acetaminophen or trimethoprim-sulfamethoxazole may

Table 2: Drug interacting with kidney radiopharmaceuticals and its outcomes

Interfering Drug	Effect on Image
Aluminum Chloride	Decreased renal distribution, and increased hepatic distribution of GHA
Sodium bicarbonate; Mannitol	Increased GHA in kidney
Captopril	In patients with hypertension and unilateral artery stenosis, there may be decreased renal uptake by the affected kidney

substantially alter the biodistribution of ^{99m}Tc-glucoheptonate) [71]. If the impact is large enough, abnormal gallbladder images may result. Affected images can mimic abnormal kidney localization on posterior views resulting in misdiagnosis [72].

Infection/Inflamation Imaging Agent

Labeled leukocytes are used to the diagnosis of lung disease, rheumatoid arthritis, detection of inflammation and a variety of other diagnostic modalities [73]. A very common problem related to labeled leukocytes in infection and inflammation diagnosis is false-negative results. This drug-interaction has been attributed to the use of antibiotics and corticosteroids. This occurs because of the reduction in the chemo-attractant stimuli for the labeled leukocytes [36]. However, other articles state that the use of antibiotics does not affect the results [74][75]. A study conducted on patients concluded that, following hip arthroplasty, non-specifically increased FDG uptake around the head or neck of the prosthesis persists for many years, even in patients without any complications [76]. Therefore, caution should be exercised when interpreting FDG uptake around the head or neck portion of prostheses with PET studies. ^{99m}Tc labeled ciprofloxacin are used for the diagnosis of bacterial infection from sterile inflammation in the body, if patient is undergone for the antibiotic or steroid therapy imaging may produce false negative or misinterpretation of the condition. It is advisable to inform patient to stopped antibiotic therapy before administration of ciprofloxacin labeled radiopharmaceutical.

Liver, Spleen and Hepatobiliary Imaging Agent

The radiopharmaceutical, ^{99m}Tc-iminodiacetic (^{99m}Tc- IDA) is used in the diagnosis of cholecystitis, focal nodular hyperplasia, degree of functional disorder in acute hepatic disease and to evaluate the severity of diffuse hepatic disease among others functions [77][78][79]. As an acid, the ^{99m}Tc-iminodiacetic acid is removed from blood by hepatocytes and subsequently transported to the gallbladder, where they are discharged through the cystic duct into the common bile duct and then into the intestine. A variety of drugs (benzodiazepine, barbiturates, opioid analgesic and antibiotics) have been reported to interfere with hepatobiliary imaging by affecting the movement of the radiopharmaceuticals through the hepatobiliary system [14]. Anti-

mycobacterial drugs isoniazid and pyrazinamide that have been shown to elevate liver enzymes and consequently affect hepatobiliary system most commonly [80]. Table 3 gives the list of the probable drugs which affect the IDA and effects of the same.

The imaging agent ^{99m}Tc-hepato-iminidiacetic acid (^{99m}Tc-HIDA) used to pancreas scintigraphy. Drugs that alter the transport in the reticuloendothelial may decrease the uptake of radiopharmaceuticals, such as ^{99m}Tc-HIDA, in the liver and spleen [14]. As such, they can lead to misdiagnosis. The impact can be quite large. A case report has been published on the complete absence of ^{99m}Tc-HIDA upon imaging, in a patient taking nicotinic acid [17]. Aluminum is present in a number of medications, most commonly in antacids. There are increasing number of case reports of interactions between aluminum and radiopharmaceuticals. Aluminum-containing drugs can cause flocculation of colloidal particles of sulfur (used in liver scanning), such that the particles get trapped in the microvasculature of the lungs decreasing the uptake of the radiopharmaceutical [81].

Thyroid Imaging Agent

The most commonly used thyroid imaging radiopharmaceuticals are (^{131}I) iodide and (^{123}I) iodide. Expansion of the iodine pool due to ingestion or parenteral administration of the iodine containing agents results in a reduced percent radioiodine uptake by the thyroid. Somatostatin also interferes with thyroid imaging through the same mechanism, absorption by receptor sites [14].

Competing anions, such as perchlorate and pertechnetate ions, act as competitive inhibitors of the iodine transport mechanism. This can lead to decreased uptake of ^{131}I sodium iodide. Inorganic iodine-containing medications such as Lugol's iodine as well as some vitamin/mineral supplements are thought to release iodine thereby decreasing the specific activity of iodide in the body pool. This would also decrease uptake of radioiodine into the thyroid gland [82][83].

Table 3: Drug interaction with IDA and outcomes of interactions

Interfering Drug	Effect on Image
Short-term chemotherapy e.g., carmustine, lomustine	a) Irregular distribution of RP in liver b) Hepatomegaly c) Shift of RP from liver to spleen and/or bone marrow
Antacids; Virulizing, Androgen therapy	Diffuse pulmonary accumulation
General anesthetic agents e.g. halothane	Shift of RP from liver to spleen
Thorium Dioxide	Absence of spleen localization
Antacids; Virulizing Androgen therapy	Diffuse pulmonary accumulation

Radioiodinated meta-iodobenzyl guanidine (^{131}I-mIBG) plays a role in both the diagnosis and treatment of a wide range of tumors; phaeochromocytoma, neuroblastoma, carcinoid tumors and medullary carcinoma of the thyroid [38][84][85][86][87]. Over 20 medicines have the potential to interfere with the biodistribution of mIBG, sometimes many hours after they have been taken. Among those, the most commonly encountered interacting agents are chlorpromazine; clomipramine, diltiazem, dopamine, fluphenazine, labetalol, nifedipine, promethazine and salbutamol [88][89]. This interference is enough to impact the efficacy of mIBG as a diagnostic and therapeutic modality because of the extremely low quantities of radiolabeled mIBG that are present in the radiopharmaceutical. Therefore, it is recommended that treatment with any potentially interacting drug be stopped one week prior to imaging with mIBG [35]. Stable iodine contained in foods (cabbage, turnip) and medications (amiodarone) can interfere with radionuclide thyroid studies [90]. Numerous noniodine containing drugs (adrenocorticotropic hormone, adrenal steroid, penicillin and bromide) also affect thyroid uptake. Thyrostatic drugs (propylthiouracil and methimazole) have modified the kinetics of radioiodine in the thyroid and through this mechanism may also have a radioprotective effect. Pre-treatment with thyrostatic medication lowers the effective half-life and uptake of radioiodine. However, this interaction also reduces the effective dose of the thyrostatic medication in the thyroid.

Discontinuation of such medications shortly before radioiodine administration can increase the absorbed energy dose in the thyroid. These drug-radiopharmaceutical interactions may also have a clinical role in lowering the effective dose of radioiodine while achieving an equally effective target dose in the thyroid [91]. Renal or liver failure and lithium will increase the thyroid uptake percentage. While it does not impact imaging, administration of non-radioactive iodine within a few days after radioiodine administration can increase the effective half-life of radioiodine in the thyroid. Therefore, its use should be suspended until few days after imaging with radioiodine, to facilitate clearance of the radioisotope.

Non-Specific Interactions

There are a number of drugs which interact across a range of radiopharmaceuticals including those used for whole body (e.g. non-organ specific) imaging. Also, drug-induced disease states can alter the biodistribution of radiopharmaceuticals [18]. For example, cytotoxic drugs such as cyclophosphamide, vincristine, and cisplatin are reported to affect the pharmacokinetic response of radiopharmaceuticals, particularly the tumor-seeking radiopharmaceutical ^{67}Ga. Antimetabolites, such as cytarabine and methotrexate, have similar effects [17]. Analogues of somatostatin (unlabeled) are used therapeutically in the Carcinoid Syndrome. There have been reports of false negative results when patients using somatostatin were imaged with ^{99m}Tc-Hynic-TOC, ^{111}In-pentetreotide, ^{68}Ga-DOTA-TATE and other receptor imaging agent due to a competition for the receptors sites [14][92]. The same will affect the therapeutic efficacy of the radiopharmaceuticals like ^{177}Lu-DOTATATE and other receptor targeting agents due to saturation of the target receptors.

Summary

Altered pharmacokinetics is one of the most common problems associated with radiopharmaceuticals which can have a significant clinical impact on safety, scan interpretation, imaging accuracy and may contributed unnecessary extra radiation dose to the patients. The present article provides an overall summary of an altered biodistribution of radiopharmaceuticals made up with different radioisotopes and related products with a special focus on the factors affecting localization and also to stimulate pharmacists to provide clinical pharmacy services to nuclear medicine.Although most drug-radio-pharmaceutical interactions are not beneficial, some nuclear medicine procedures are conducted in presence of drug intervention to enhance the diagnostic efficacy of the test and reduce the radiation toxicity. This review provides organ wise summary of various aspects that can indicate possible interaction between drug and radiopharmaceuticals and highlights factors to exemplify the significance of altered pharmacokinetics of radiopharmaceuticals in the tabulated form to allow the easy access of source material. Manufacturer and suppliers of the radiopharmaceuticals (BRIT, Navi Mumbai) enlist and provide the list of drugs/food which have probable interaction with the radiopharmaceuticals along with respective cold kit and any interaction found by the user should be informed to the BRIT to update. This will help as a guidance document (ready reckoner) to the nuclear medicine fraternity in India to avoid interactions.

References

1. Ruiz-Laiglesia, F. J., Oliveira-Gonzalez, S., and Torrubia-Pérez, C. B. 'Diagnostic limitations of positron emission tomography. What are we seeking?' Rev. Clin. Esp. 208 (2008) 87–89.

2. Shaw S. M. 'Drugs and diseases that may alter the biodistribution or pharmacokinetics of radiopharma-ceuticals'. Pharm Internat. 6 (1985) 293-298.

3. Zhao, Y., and Wang, Q. 'Bone uptake of ^{99m}Tc-MIBI in patients with hyperparathyroidism'. Ann. Nucl. Med. 28 (2014) 349-355.

4. Mozayani, A., and Raymon, L. P, 'Handbook of Drug Interactions A Clinical and Forensic Guide'. Mozayani, A. and Raymon, L. P. (Eds.), Human Press Inc., Totowa, New York, (2004) pp. v-vi.

5. Greenblatt, D. J., and Moltke von, L. L. 'Drug-Drug Interactions', A. D. Rodrigues, Ed., Drug-Drug Interactions: Clinical Perspective; 2nd edition; (2008) pp 643.

6. Kvasz M, Allen I E, Gordon M J, Ro E Y, Estok R, Olkin I and Ross S. 'Adverse drug reactions in hospitalized patients: a critique of a meta-analysis'. Gen. Med. 2 (2000) E3.

7. Drugs and Cosmetic Act 1940 and Rules 1945, “Schedule K” Govt. of India, An Act to regulate the import,

manufacture, distribution and sale of drugs.(1940) p 380.

8. Indian Pharmacopoeia, Government of India, Ministry of health and family welfare, (2014).

9. Kusabe K, Okamura T, Kasagi K, Komatani A, Sato Y, Matsuda H and Maruno H. Subcommittee for Safety Issues of Radiopharmaceuticals, Medical Science and Pharmaceutical Committee, Japan Radioisotope Association. [The 27th Report on Survey of the Adverse Reaction to Radiopharmaceuticals (the 30th survey in 2004)] Kaku Igaku, 43 (2006) 23–35.

10. Hesslewood S. and Keeling D. H. 'Frequency of adverse reactions to radiopharmaceuticals in Europe'. Eur. J. Nucl. Med. 24 (1997) 1179–1182.

11. Cordova M A, Rhodes B A, Atkins H L, Glenn H J, Hoogland D R and Solomon A C. 'Adverse reactions to radiopharmaceuticals'. J. Nucl. Med. 23 (1982) 550–551.

12. Silberstein E B and Ryan J. 'Prevalence of adverse reactions in nuclear medicine'. J. Nucl. Med. 37 (1996) 185–192.

13. Keeling D H. 'Adverse reactions and untoward events associated with the use of radiopharmaceuticals'. In: Sampson C B (Ed.), Textbook of radiopharmacy theory and practice. Yverdon: Gordon and Breanch Science Publishers, (1994) pp. 285–295.

14. Hesslewood S and Leung E. 'Drug interaction with radiopharmaceuticals'. Eur. J. Nucl. Med. 21 (1994) 348–356.

15. Sampson C B and Hesslewood S R. 'Altered biodistribution of radiopharmaceuticals as a result of pharmacological or chemical interaction'. J. Biopharm. 5 (1989)131–151.

16. Radiation in Medicine: A Need for Regulatory Reform; Institute of Medicine, Chapter 3; Regulation and Radiation Medicine, 14 (1995) pp 82.

17. Sampson C B. 'Adverse reactions and drug interaction with radiopharmaceuticals'. Drug safety 8 (1993) 280–294.

18. Sampson C B. 'Drugs and chemicals which affect the purity, biodistribuition and pharmacokinetics of radiopharmaceuticals'. J. Biopharm. Sci. 1 (1990) 381–400.

19. Callahan R J and Rabito C A. 'Radiolabeling of erythrocytes with ^{99m}Tc: role of band-3 protein in the transport of pertchnetate across the cell membrane. J Nucl Med, 31(1990) 2004–10.

20. Fisher S M, Brown R G and Greyson N D. 'Unbinding of ^{99m}Tc- by iodinated antiseptics. J. Nucl. Med. 18 (1977) 1139–1140.

21. Slater D M, Anderson M and Garvie N W. 'Syringe extractables, effects on radiopharmaceuticals'. Lancet, 17 (1983) 1431–1432.

22. Millar A M, Wathem C J and Muir A L. Failure in labeling of red cells with ^{99m}Tc: interaction between intravenous cannulae and stannous pyrophosphate. Eur. J. Nucl. Med. 8 (1983) 502–504.

23. Vidal M V, Gutfilen B, Da Fonseca L M and Bernardo-Filho M. 'Influence of tobacco on the labeling of red blood cells and plasma proteins with ^{99m}Tc'. J. Exp. Clin. Cancer Res. 17 (1998) 41–46.

24. Jones J K. 'Adverse drug reactions in the community health setting: approaches to recognizing, counseling and reporting'. Fam. Comm. Health, 5 (1982) 58–67.

25. Vallabhajosula S, Killeen R P and Osborne J R. 'Altered biodistribution of radiopharmaceuticals: role of radiochemical/pharmaceutical purity, physiological and pharmacologic factors'. Seminars in Nucl. Med. 40 (2010) 22.

26. Hladik W B, Nigg K K, Rhodes B A. 'Drug-induced changes in the biologic distribution of radiopharmaceuticals'. Semin. Nucl. Med. 12 (1982) 184-210.

27. Laven D L, Shaw S M. 'Detection of drug interactions involving radiopharmaceuticals: a professional responsibility of the clinical pharmacist'. J. Pharm. Pract. 2/5 (1989) 287-298.

28. Verhoeff N P L G. 'Pharmacological implications for neuroreceptor imaging'. Eur. J. Nucl. Med. 18 (1991) 482–502.

29. Lentle B C and Scott J R. 'Iatrogenic alterations in radionuclide biodistribution'. Semin. Nucl. Med. 9 (1979) 131–134.

30. Hawkins R A and Biebuyck J F. 'Ketone bodes are selectively used by individual brain regions'. Science 205 (1979) 325-327.

31. Van Leeuwen-Stok E A, Jonkhoff A R, Visser-Platier A W, Dräger L M, Teule G J, Huijgens P C and Schuurhuis G J. 'Cell cycle dependency of ^{67}Ga uptake and cytotoxicity in human cell-lines of hematological malignancies'. Leukemia Lymphoma, 31 (1998) 533–544.

32. Waxman A S, Beldon J R, Richli W R, Tanasescu D E and Siemsen J K. 'Steroid induced suppression of gallium uptake tumors of the central nervous system'. J. Nucl. Med. 18 (1997) 617.

33. Moreno S R F, Carvalho J J, Nascimento A L, Pereira M, Rocha EK, Olej B, Caldas L Q A and Bernardo-Filho M. 'Experimental model to assess possible medicinal herb interaction with a radiocomplex: Qualitative and quantitative analysis of kidney, Liver and duodenum isolated from treated rats'. Food Chem Toxicol, 45 (2007b) 19–23.

34. Rodriguez J S, Varela L G, Arias E L, Prado I D, Cortes J, Montero J P,

FerreiroA F, Ruibal A, Sobrino T. Aguiar P. 'Impact of benzodiazepines on brain FDG-PET quantification after single-dose and chronic administration in rats'. Nucl. Med. Bio, 43/12 (2016) 827–834.

35. Solanki K K, Bomanji J, Moyes J, Mather S J, Trainer P J and Britton K E. 'A pharmacological guide to medicines which interfere with the biodistribution of radiolabelled meta-iodobenzyl-guanidine (mIBG)'. Nucl. Med. Commun. 13 (1992) 513–521.

36. Hladik W B, Ponto J A, Lentle B C and Laven D L. 'Iatrogenic alterations in the biodistribution of radiotracers as a result of drug therapy: reported instances'. In: Hladik W B, Saha G B and Study K T (Eds.), Essentials of Nuclear Medicine Science. Williams and Wilkins: Sydney, Baltimore. (1987) pp189–219.

37. Fischer M, Vetter W and Winter B. 'Adrenal scintigraphy in primary aldosteronism. Spironolactone as a cause of incorrect classification between adenoma and hyperplasia'. Eur. J. Nucl. Med. 7 (1972) 222–224.

38. Fischer M, Winterberg B and Muller-Rensing R. 'Radioisotopic therapy of pheochromocytoma'. Nucl. Compact. 14 (1983) 172–176.

39. Khafagi F A, Shapiro B and Gross M D. 'The adrenal gland apud', In: Maisey M N, Britton K E and Gilday D L (Eds.) Clinical Nuclear Medicine, Chapman and Hall: London, (1991) pp. 271–291.

40. Gross M D, Valk T W, Sawanson D P, Thrall J H, Grekin R J and Beirewaltes W H. 'The role of pharmacologic manipulation in adrenal cortical scintigraphy'. Semin. Nucl. Med. 11 (1981) 128–148.

41. Bardet S. '131-6-Iodomethylnor-cholesterol scinti-graphy: an assessment of its role in the investigation of adrenocortical incidentalomas'. Clin. Endocrinol. 44 (1996) 587–596.

42. Mansmann G, Lau J, Balk E, Rothberg M, Miyachi Y and Bornstein S R. 'The clinically inapparent adrenal mass: update in diagnosis and management'. Endocr. Rev. 25 (2004) 309–340.

43. Swanson D P, Chilton H M and Thrall J H. Pharmaceuticals in medical imaging. 6th Edn., New York: Macmillan (1990) pp 1–100.

44. Sandler E D, Parisi M T and Hattner R S. 'Duration of etidronate effect demonstrated by serial bone scintigraphy'. J. Nucl. Med. 32 (1991) 1782–1784.

45. Hommeyer S H, Varney D M and Eary J F. 'Skeletal non-visualization in a bone scan secondary to intravenous etidronate therapy'. J. Nucl. Med. 33 (1992) 748–750.

46. Crawford J A and Gumeran L W. 'Alteration of body distribution of ^{99m}Tc-pyrophosphate by radiographic contrast material'. Clin. Nucl. Med. 3 (1978) 305–307.

47. Forauer A R, Grossman S J and Joyce J M. 'Altered biodistribution of ^{99m}Tc-HMDP on bone scintigraphy from recent intravenous iron therapy'. Clin. Nucl. Med. 19 (1994) 817–818.

48. Eisenberg B, Meholic A J, Arrington E R, Elliott T M, Wiest P W and Olander R L. 'Iron dextran: bone imaging patterns of absorption – a case report'. Am. J. Physiol. Imag. 5 (1990) 116–118.

49. Mazzole A C, Barker M M and Belliveal R E. 'Accumulation of ^{99m}Tc-diphosphonate at sites of intramuscular iron therapy'. J. Nucl. Med. Tech. 4 (1976) 133–135.

50. Van Der Wall E E, Westera G, Van Eenige M J, Scholtalbers S, Visser F C, Den Hollander W and Roos J P. 'Influence of propranolol on uptake of radioiodinated heptadecanoic acid and ^{201}Tl in the dog heart'. Eur. J. Nucl. Med. 8 (1983) 454–457.

51. Bridges A B, Kennedy N, Mcneill G P, Cook B and Pringle T H. 'The effect of atenolol on dipyridamole ^{201}Tl myocardial perfusion tomography in patients with coronary artery disease'. Nucl. Med. Commun. 13 (1992) 41–46.

52. Miyagawa M, Tanada S and Hamamoto K. 'Scintigraphic evaluation of myocardial uptake of ^{201}Tl and ^{99m}Tc-pyrophosphate utilizing a rat model of chronic doxorubicin cardiotoxicity'. Eur. J. Nucl. Med. 18 (1991) 332–338.

53. Yurekli Y, Unak P, Ertay T, Biber Z, Medine I and Teksoz S. 'Radio-pharmaceutical model using ^{99m}Tc-MIBI to evaluate amisfostine protection against doxorubicin cardiotoxicity in rats'. Ann. Nucl. Med. 19 (2005) 197–200.

54. Narahara K A, Thompson C J, Hazen J F, Brizendine M and Mena I. 'The effect of beta-blockade on single photon emission computed tomographic (SPECT) ^{201}Tl images in patients with coronary disease'. Am. Heart J. 117 (1989) 1030–1035.

55. Chacko A K, Gordon D H, Bennet J M, O'Mara R E and Wilson G A. 'Myocardial imaging with ^{99m} Tc-pyrophosphate in patients on adriamycin treatment for neoplasia'. J. Nucl. Med. 18 (1997) 680–683.

56. Hegge F N, Hamilton G W and Larson S M. 'Cardiac chamber imaging: a comparison of red blood cells labelled with ^{99m} Tc, in-vitro and in-vivo'. J. Nucl. Med. 19 (1978) 129–134.

57. Hilliard N, Presented at Southwest Chapter of Society of Nuclear Medicine Meeting, Little Rock, Arkansas, Mar 29, (2008).

58. Estorch M, Carrio I, Berna L, Martinez-Duncker C, Alonso C, Gérman J P and Ojeda B. '^{111}In-antimyosin scintigraphy after doxorubicin therapy in patients with advanced breast cancer'. J. Nucl. Med. 31 (1990) 1965–1969.

59. Reuland P, Ruck P and Feine U. 'Correlation of chemotherapy-induced

kidney disorder and antimyosin antibody uptake in kidneys'. J. Nucl. Med. 33 (1992) 309–311.

60. Lopez M and Vici P. 'European trials with dexrazoxane in amelioration of doxorubicin and epirubicin-induced cardiotoxicity'. Semin. Oncol. 25 (1998) 55–60.

61. Carrio I, Lopez-Pousa J and Marinez-Duncker D. 'Comparison of cardiotoxicity by ^{111}In-antymyosin studies: bolus administration versus continuous infusion of doxorubicin'. Eur. J. Nucl. Med. 20 (1993) 833–834.

62. Pauwels E K J, Feitsma R I J, Blom J. 'Influence of adriamycin on red blood cell labelling; A pitfall in scintigraphic blood pool imaging'. Nucl. Med. Commun. 4 (1983) 290–295.

63. Sheng Y, Bryngelsson C and Pero R W. 'Enhanced DNA repair, immune function and reduced toxicity of c-med-100, a novel aqueous extract from Uncariatomentosa'. J. Ethnopharmacol. 69 (2000) 115–126.

64. Williams J E. 'Review of antiviral and immunomodulating properties of plants of the Peruvian rain forest with a particular emphasis on uña de gato and sangre de grado'. Altern. Med. Rev. 6 (2001) 567–579.

65. Moreno S R F. 'Effect of oral ingestion of an extract of the herb uncaria tomentosa on the biodistribution of sodium pertechnetate in rats'. Braz. J. Med. Biol. Res. 40 (2007a) 77–80.

66. Israel O, Weiler-Sagie M, Rispler S, Bar-Shalom R, Frenkel A, Keidar Z, Bar-Shalev A and Strauss H W. 'PET/CT quantification of the effect of patient-related factors on cardiac ^{18}F-FDG uptake'. J. Nucl. Med. 48 (2007) 234–239.

67. Bouchelouche K and Oehr P. 'Positron emission Tomography and positron emission tomography/computerized tomography of urological malignancies: an update review'. Urol, 179 (2008) 34–35.

68. Claveau-Tremblay R, Turpin S, De Braekeleer M, Brassard A and Leblond R. 'False-positive captopril renography in patients taking calcium antagonists'. J. Nucl. Med. 39 (1998) 1621–1626.

69. Latham T B, Prato F S, Wisenberg G and Reese L. 'Effects of dipyridamole infusion on human renal function observed using ^{99m}Tc-DTPA'. J. Nucl. Med. 33 (1992) 355–358.

70. Gomes M L, Mattos D M M, Souza-Freitas R, Bezerral R J and Bernardo-Filho M. 'Study of the toxicological effect of mitomycin-c in mice: alteration on the biodistribution of radiopharmaceuticals used for renal evaluations'. Hum. Exp. Toxicol. 20 (2001) 193–197.

71. Web page accessed on March 2021 http://www.uspharmacist.com/oldformat.asp?url=newlook/files/feat/mar00druginteractions.htm Retrieved on 9 Nov (2020).

72. Hinkle G H, Basmandjian G P, Peek C, Baker K K and Ice R D. 'Effects of

concurrent drug therapy on ^{99m}Tc-Gluceptate biodistribution'. Am. J. Hosp. Pharm. 39 (1982) 1930–1933.

73. Van Hemert F J, Thurlings R, Dohmen S E, Voermans C, Tak P P, Van Eck-Smit B L and Bennink R J. 'Labelling of autologous monocytes with ^{99m}Tc-HMPAO at very high specific radioactivity'. Nucl. Med. Biol. 34 (2007) 933–938.

74. Chung C J, Hicklin O A, Payan J M and Gordon L. '^{111}In-labelled leukocyte scan in detection of synthetic vascular graft infection: the effect of antibiotic treatment'. J. Nucl. Med. 32 (1991) 13–15.

75. Datz F L and Thorne D A. 'Effect of antibiotic therapy on the sensitivity of ^{111}In-labelled leukocyte scans'. J. Nucl. Med. 27 (1986) 1849–1853.

76. Zhuang H, Chacko T K, Hickeson M, Stevenson K, Feng Q, Ponzo F, Garino J P and Alavi A. 'Persistent non-specific ^{18}F-FDG uptake on PET imaging following hip arthroplasty'. Eur. J. Nucl. Med. 29 (2002) 1328–1333.

77. Alobaidi M, Gupta R, Jafri S and Fink-Bennet D. 'Current trends in imaging evaluation of acute cholecystitis'. Emerg. Radiol. 10 (2004) 256–258.

78. Aburano T, Yokoyama K, Shuke N, Takayama T, Michigishi T, Tonami N, Hisada K, Unoura M and Kobayashi K. '^{99m}Tc colloid and ^{99m}Tc IDA imaging in diffuse hepatic diseases'. J Clin Gastroenterol 17 (1993) 321–326.

79. Broglia L, Bezzi M, Massa R, Tortora A, Rossi M, Prosperi D, Maccioni F and Rossi P. 'Computerized tomography, magnetic resonance and nuclear medicine in the non-invasive diagnosis of focal nodular hyperplasia of the liver'. Radiol. Med. 96 (1998) 218–225.

80. Pv K, Palaian S and Pr S. 'Pattern of adverse drug reactions experienced by tuberculosis patients in a tertiary care teaching hospital in western Nepal.' Pak J Pharm Sci, 21 (2008) 51–56.

81. Bobinet E B, Severin M and Zurbriggen M T. 'Lung uptake of ^{99m}Tc-Sulphur Colloid in patients exhibiting presence of aluminum in plasma'. J. Nucl. Med. 15 (1974) 1120–1122.

82. Sternthal E, Lipworth L, Stanley B, Abreau C, Fang S L and Braveman L E. 'Supression of thyroid radioiodine uptake by various doses of stable Iodine'. N. Engl. J. Med. 303 (1980) 1083–1088.

83. Laurie A J, Lyon S G and Lasser E C. 'Contrast material Iodides: potential effects on radioactive Iodine thyroid uptake'. J. Nucl. Med. 33 (1992) 237–238.

84. Sone T, Fukunaga M, Otsuka N, Morita R, Muranaka A, Yanagimoto S, Tomomitsu T, Nakayama H and Harada T. 'Metastatic medullary thyroid cancer, localization with ^{131}I-mIBG'. J. Nucl. Med. 26 (1985) 604–608.

85. Sisson J C, Frager M S, Valk T W, Gross M D, Swanson D P, Wieland D

M, Tobes M C, Beierwaltes W H and Thompson N W. Scintigraphic localization of pheochromocytoma. N Eng J Med, 305 (1981) 12–17.

86. Horne T, Hawkings L A and Britton K E. 'Imaging of phaeochromocytoma and adrenal medulla with ^{123}I-metaiodobenzylguanidine'. Nucl. Med. Commun. 5 (1984) 763–768.

87. Kimming B, Brandeis We, Eisenhut M, Bubeck B, Hermann H J and Winkel K. 'Scintigraphy of neuroblastomas with ^{131}I-mIBG'. J. Nucl. Med. 25(1984) 773–775.

88. Bombardieri E. Giammarile F, et al. ^{131}I/^{123}I-metaiodobenzylguanidine (mIBG) scintigraphy: procedure guidelines for tumour imaging'. Eur. J. Nucl. Med. Mol. Imaging, 37 (2010) 2436-2446.

89. Khafagi F A, Shapiro B, Lorraine M, Mallette S and Sisson J C. 'Labetolol reduces ^{131}I-mIBG uptake by pheochromocytoma and normal tissues'. J. Nucl. Med. 30 (1989) 481–489.

90. Ziessman H A, O'Malley J P, Thrall J H, 'Nuclear Medicine: The Requisites in Radiology', In: Endocrine System, 3rd Edn,, Elsevier, Mosbey(2006) 71-112.

91. Moka D, Dietlein M, Schicha H. 'Radioiodine therapy and thyrostatic drugs and iodine'. Eur. J. Nucl. Med. Mol. Imag. 29 (2002) 486–491.

92. Dorr U, Rath U, Sauter-Bihl M-L, Guzman G, Bach D, Adrian HJ and Bihl H. 'Improved visualization of carcinoid liver metastases by ^{111}In-Pentetreotide scintigraphy following treatment with cold somatostatin analogue'. Eur. J. Nucl. Med. 20 (1993) 431–433.

Actinium-225: What do we know so far about the rarest drug on our planet?

Dheeraj Kumar

[1]**Radiopharmaceutical Laboratory (RPL), BRIT Vashi Complex**

(Corresponding author:dheeraj.kum@britatom.gov.in)

Abstract

The alpha emitter actinium-225 (^{225}Ac) is an extremely promising radioisotope for applications in targeted alpha therapy of cancer and infectious diseases. Currently, the worldwide availability of ^{225}Ac for research and clinical trials is very limited, and only a few commercial suppliers exist in the USA, Canada, and Europe. The present review describes, in brief, the current status of ^{225}Ac. The review summarizes, in brief, the various methods that are presently in practice or being pursued world-over to produce ^{225}Ac. A clinical trial result is also included in the introduction section to demonstrate the vastly improved efficacy of ^{225}Ac-based radiopharmaceuticals in comparison to the conventional therapeutic modalities.

Keywords: *Targeted radionuclide therapy (TRT), targeted alpha therapy (TAT), alpha emitter, ^{233}U, ^{225}Ac, ^{227}Ac, ^{226}Ra, ^{223}Ra, ^{212}Bi, ^{213}Bi, ^{212}Pb, ^{226}Th, ^{227}Th, ^{211}At*

Introduction

In the past decade, there is a dramatic increase in the interest in targeted radionuclide therapy (TRT). The primary reason for this increased interest is the ever-growing clinical evidence of the value of targeted alpha therapy (TAT) in the treatment of acute myeloid leukemia (AML), melanomas, carcinomas, and various other oncological diseases as well as infectious diseases. TAT utilizes alpha emitters bound to monoclonal antibodies (mAbs), peptides, or small molecules for targeting the tumor cells.

Recently, this therapeutic regimen has gained significant popularity world-over. This increased popularity can be attributed to the combined effects of (a) advancements in technology in the last few decades that helped researchers in identifying new in vivo targets, (b) novel synthetic approaches, and (c) increased availability of alpha emitters of significance[1].

Alpha emitting Radionuclides

Alpha emitting radionuclides or alpha emitters as they are popularly called are the most potent radionuclides for the treatment of metastatic cancers. They have high linear energy transfer (LET) values (close to 100 keV/μm) and short-range in tissue (approx. 50-100 μm). Consequently, they can deliver large radiation doses over a few cell diameters. Thus, alpha emitters effect unparalleled cytotoxicity when targeted to cancer, while minimizing damage to surrounding healthy tissue, owing to their short range in tissues. A few examples of alpha emitters of significance in nuclear medicine include *^{223}Ra, ^{212}Bi, ^{213}Bi, ^{211}At, ^{212}Pb, ^{225}Ac, ^{226}Th, ^{227}Th, etc.*

The nuclear characteristics of these alpha emitters are listed below in Table 1[2]

Table 1: Nuclear characteristics of alpha emitters

S NO	Radionuclide	Daughter Isotope	Half-life	Emission (%)	Energy
1	**^{225}Ac**	**^{221}Fr**	**9.92 days**	**α (100 %)**	**5.776 MeV**
2	^{211}At	^{207}Bi	7.214 hours	α (41.80 %)	2.454 MeV
3	^{212}Bi	^{208}Tl	60.55 minutes	α (35.94 %)	2.175 MeV
4	**^{213}Bi**	**^{213}Po**	**45.59 minutes**	**β^- (97.86 %)**	**0.426 MeV**
		^{209}Tl	**45.59 minutes**	**α (2.14 %)**	**5.905 MeV**
5	^{212}Pb	^{212}Bi (further decay by α particle emission)	10.622 hours	β^- (100 %)	0.101 MeV (β^-) + 2.175 MeV (from Bi-212 decay)
6	^{223}Ra	^{219}Rn	11.43 days	α (100 %)	5.629 MeV
7	^{226}Th	Ra	30.57 minutes	α (100 %)	6.306 MeV
8	^{227}Th	^{223}Ra	18.697 days	α (100 %)	5.901 MeV

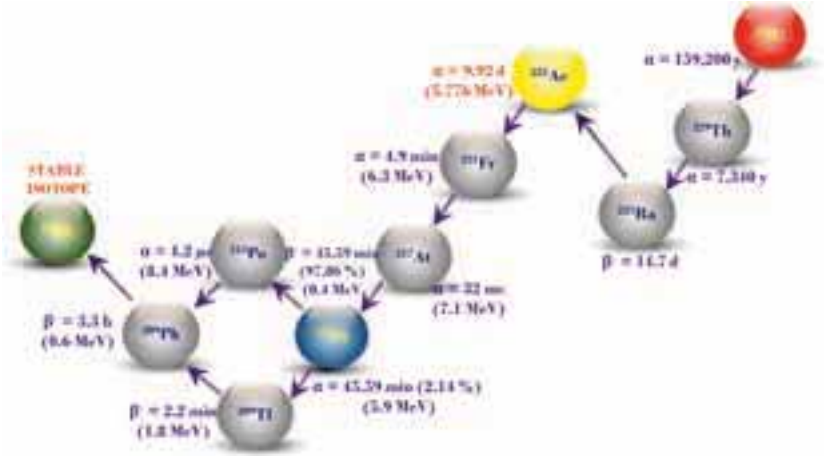

Fig. 1: ^{225}Ac formation and its sequential decay to stable isotope ^{209}Bi through 4 net α-emissions per decay[2, 4]. The sequential α-emissions, associated with the release of large amounts of energies in the MeV range make therapy with ^{225}Ac extremely beneficial.

Out of the alpha-emitting radionuclides mentioned, ^{225}Ac and its daughter product Bismuth-213 are of considerable interest for use in targeted alpha therapy because of their short half-lives and associated high energy radiation capable of effecting double strand breakage of DNA in a tumor cell. Between ^{225}Ac and its daughter ^{213}Bi, the former with an almost 300-fold larger half-life (10 d) and 4 alpha particle emissions per decay has displayed better in vitro cytotoxicity, and thereby much lower LD_{50} value, making it a radioisotope of choice in nuclear medicine applications[3]. Nevertheless, ^{213}Bi is a promising radioisotope for TAT and can be obtained from the decay of ^{225}Ac, thus ^{225}Ac/^{213}Bi generators are currently being pursued by many researchers for use in therapeutic applications. The formation of ^{225}Ac and ^{213}Bi from ^{233}U and their sequential decay to stable isotope ^{209}Bi is shown below in Fig. 1.

Extensive clinical trials are being performed in the US, Europe, and other developing countries to study the therapeutic effect of ^{225}Ac- and ^{213}Bi-based radiopharmaceuticals in brain tumors, leukemia, lymphoma, melanoma, gastric, prostate, ovarian, and pancreatic cancers. Preliminary clinical trial data have shown that ^{225}Ac-based radiopharmaceuticals cause remission even in those cancer patients who have exhausted all other conventional therapeutic modalities.

Fig. 2 below, shows the clinical trial results for a patient who did not respond to the conventional ^{177}Lu-PSMA-617 therapy, however, the patient showed almost complete remission with only 4 cycles of ^{225}Ac-PSMA-617 radiopharmaceutical[5].

This success story is one of the many examples of the clinical advantages of ^{225}Ac-based alpha therapy over conventional therapeutic modalities.

Production Routes of Actinium-225 (^{225}Ac)

^{225}Ac can be produced in both reactors as well as accelerators. It can also be separated from legacy wastes of ^{233}U. Some of the production routes of ^{225}Ac are mentioned in Table 2 below. Some of the methods have significant disadvantages associated with processing and hence are rarely used.

[I] Production route 1: Production of the parent radioisotope ^{229}Th in high flux nuclear reactors by sequential neutron

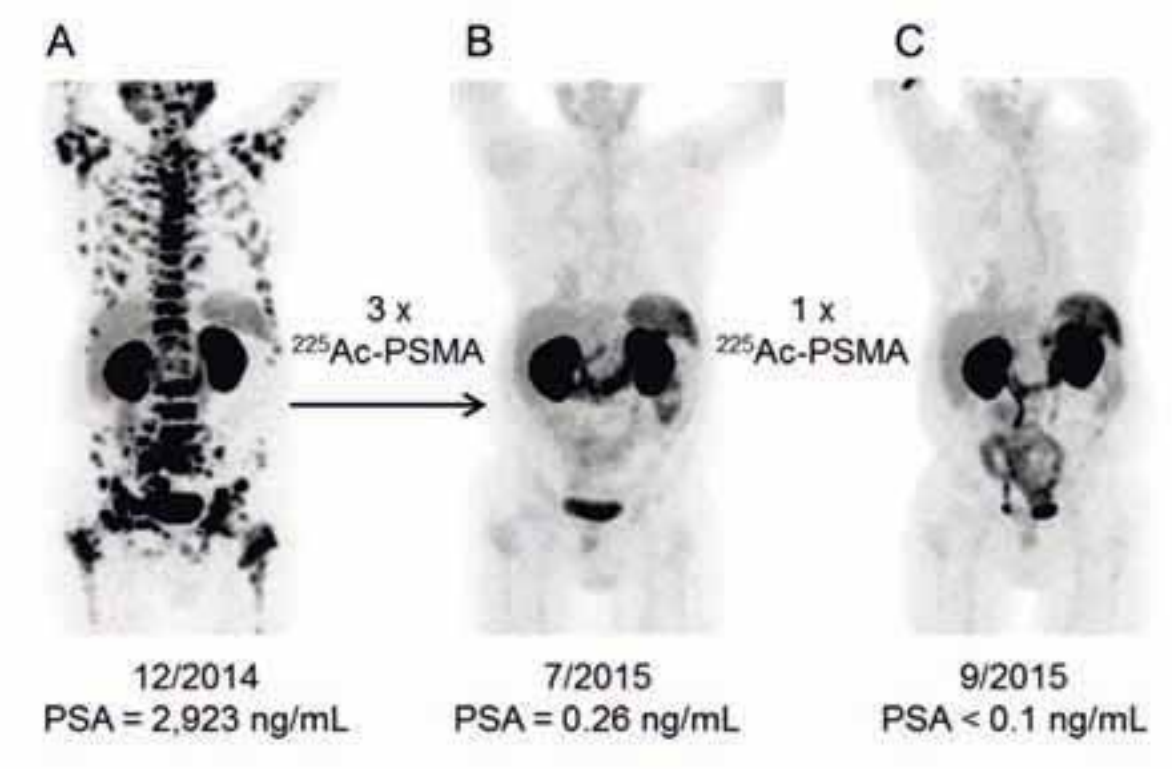

Fig. 2: ^{68}Ga-PSMA-11 PET/CT-scan. (A) Pre-therapeutic tumor spread scan taken after ^{177}Lu-PSMA-617 cycle (B) restaging 2 months after the third cycle of ^{225}Ac-PSMA-617 (C) and 2 months after one additional consolidation therapy (Reproduced with permission) (PSA = prostate specific antigen)[5].

capture of ^{226}Ra (Scheme 1 of Table 2)

$^{226}Ra(n,\gamma)^{227}Ra(n,\gamma)^{228}Ra(n,\gamma)^{229}Ra \rightarrow {}^{229}Ac \rightarrow {}^{229}Th \rightarrow {}^{225}Ac$

When ^{226}Ra is irradiated in a high flux reactor, ^{229}Th is produced by sequential capture of neutrons in the radium target as shown in Table 2. However, due to the sequential neutron capture route, ^{228}Th is also produced. As a matter of fact, at equilibrium, the concentration ratio of ^{228}Th to ^{229}Th is about 1:1. One of the daughter products in the decay chain of ^{228}Th is ^{208}Tl, which is a hard gamma emitter (E = 2.2 MeV). Therefore, very heavy shielding is required to process irradiated targets containing ^{228}Th, which limits the quantity of ^{229}Th that can be processed in the hot cell in a batch. Therefore, ^{225}Ac yield per batch after purification is generally low (less than 10 mCi) [6].

[II] Production route 2: (Scheme 1 of Table 2)

$^{228}Ra(n, \gamma)\ {}^{229}Ra \rightarrow {}^{229}Ac \rightarrow {}^{229}Th \rightarrow {}^{225}Ac$

This route follows the same scheme as that of production route 1, but the target is ^{228}Ra instead of ^{226}Ra. One of the daughter products of the ^{232}Th cycle is ^{228}Ra ($t_{1/2}$ = 5.76 y), during the processing of ^{232}Th, ^{228}Ra is isolated in high yields. This can then be irradiated in nuclear reactors for the production of ^{229}Th. However, due to the high buildup of ^{228}Th during target preparation, irradiation, and processing, again shielding problems same as mentioned in route 1 are encountered and ^{225}Ac is obtained in low yield [6].

[III] Production route 3: (Scheme 2 of Table 2, production using LINAC)

$^{226}Ra(\gamma, n)\ {}^{225}Ra \rightarrow {}^{225}Ac$

In a linear accelerator (LINAC), an electron gun at the cathode emits a steady stream of electrons in a drift tube, where they are attracted towards an anode at the other end. This mono-energetic high-energy pulsed electron beam then strikes the target (usually tungsten) releasing energy in the form of Bremsstrahlung. The

Table 2: Different production routes of actinium-225.Note: ^{229}Th decays by α-emission to ^{225}Ac

S No	Production route	Associated Nuclear Reaction
1	Nuclear Reactor (thermal neutrons)	$^{226}Ra(n, \gamma)^{227}Ra(n, \gamma)^{228}Ra\ (n, \gamma)\ {}^{229}Ra \rightarrow {}^{229}Ac \rightarrow {}^{229}Th$
2	Accelerator (electrons)	$^{226}Ra(\gamma, n)\ {}^{225}Ra \rightarrow {}^{225}Ac$
3	Accelerator (low energy particles)	$^{226}Ra\ (p,2n)\ {}^{225}Ac$ $^{226}Ra\ (\alpha,2n)\ {}^{225}Ac$ $^{226}Ra\ (p, pn)\ {}^{225}Ra \rightarrow {}^{225}Ac$ $^{232}Th\ (p, x)\ {}^{229}Th$
4	Accelerator (high energy particles)	$^{232}Th\ (p, x)\ {}^{225}Ac$ $^{232}Th\ (p, x)\ {}^{225}Ra \rightarrow {}^{225}Ac$
5	Accelerator (high energy neutrons)	$^{226}Ra\ (n,2n)\ {}^{225}Ra \rightarrow {}^{225}Ac$
6	Hot cell facility	^{229}Th decay to ^{225}Ac

photons generated in Bremsstrahlung have a distribution over a wide range (from zero to maximum electron beam energy). This photon spectrum is utilized to bombard ^{226}Ra. If the photon energy is greater than 6.4 MeV, it is sufficient to remove a neutron from ^{226}Ra leaving behind ^{225}Ra. ^{225}Ra then undergoes natural beta decay ($t_{1/2} = 14.9$ d) to ^{225}Ac.

Thus, for routine production of ^{225}Ac, 20 mg of ^{226}Ra is irradiated for sufficient time (production rate of ^{225}Ac is limited to 66 μCi per hour with 18 MV x-rays). After irradiation, the target is cooled for nearly 18 days. After around 18 days, ^{225}Ac and ^{225}Ra achieve transient equilibrium, and the ^{225}Ac (peak activity) is separated. The maximum achievable activity of ^{225}Ac is 44.06 % of ^{225}Ra formed during irradiation of ^{226}Ra[7]. The ^{226}Ra recovered can be sent for the next irradiation cycle.

[IV] Production route 4: (Scheme 3 of Table 2, cyclotron production route of Ac-225)

^{226}Ra (p, 2n) ^{225}Ac

In this route of production, $RaCl_2$ is mixed with large quantities of $BaCl_2$, which is suitably chosen as a matrix because Ba and Ra have similar chemical properties. The target is loaded in a silver capsule and welded gas tight. The silver capsules are then irradiated in a cyclotron having proton beam energy 8-28 MeV and beam current 10-50μA[8]. Since irradiation is done by proton beam, target cooling is required, and the silver capsules are water-cooled. The maximum cross-section for (p,2n) reaction is observed around ~16 MeV and thus ^{225}Ac in high yield can be obtained by low energy level III medical cyclotrons operating in large numbers worldwide. A schematic of the target design for proton beam irradiation of $^{226}RaCl_2$ is shown below in Fig. 3.

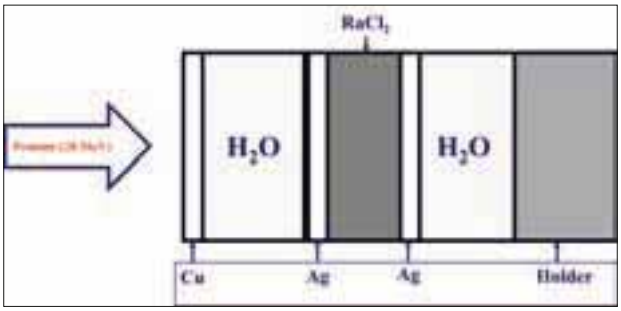

Fig. 3: Schematic view of target design utilized for $RaCl_2$ irradiation; the target has provision for water cooling (redrawn from Reference[8]).

Post irradiation, the target is cooled for 2-3 days, dissolved in 0.01 M HCl, and purified by a series of extraction chromatographic resins (Ln-spec resin and Sr-spec resins).

[V] Production route 5: (Scheme 4 of Table 2, Spallation of ^{232}Th)

^{232}Th (p, x) ^{225}Ac

A very efficient route of producing ^{225}Ac is via spallation of ^{232}Th by extremely high energy proton beams. Spallation is a type of nuclear reaction in which a high-energy particle or photon hits a nucleus and causes it to emit many other particles or photons. In spallation, the binding energy of the compound nucleus, formed after combining with high energy projectile, is very high and it breaks into many fragments. Therefore, the higher the energy of the proton beam, the higher number of fragments formed. Very high yields of ^{225}Ac are obtained when ^{232}Th is irradiated with a proton beam of energy 200 MeV and higher. At constant beam

currents, yields increase with proton energy up to 400 MeV and then decrease slightly thereafter. While ^{225}Ac is produced in a very high yield during this process, purification of ^{225}Ac from a such large number of spallation products is a challenging task. The target utilized is sheets of natural thorium, which are encased in a copper enclosure. Post fabrication, the targets are irradiated in a steady beam of approximately 2.5 x 10^{16} protons per day for 5 days. Since the spallation event gives rise to a large number of fragments along with ^{225}Ac, the target is cooled for at least 10 days to decay the short-lived isotopes and then processed utilizing a modified version of ion-exchange and extraction chromatography with the use of AGMP-1 resin (ion exchanger) and DGA and UTEVA resins (extraction chromatographic resins)[9].

A disadvantage of this route is the co-production of ^{227}Ac in the target material in a ratio of 1000:1 (^{225}Ac:^{227}Ac). ^{227}Ac has a half-life of 21.77 years, which makes the use of ^{225}Ac contaminated with ^{227}Ac in patients difficult. As a consequence, there is a severe constraint on the radio-nuclidic purity of ^{225}Ac. A typical clinical dose of ^{225}Ac for use in human patients (average 70-80 kg) is approximately 10 MBq (approx. 270 μCi), and in Germany, the general exemption level of ^{227}Ac in ^{225}Ac for use in patients is 1kBq (not more than 0.0001 % of ^{225}Ac).

[VI] Production route 6: (Scheme 6 of Table 2, from the legacy waste of ^{233}U)

Although ^{225}Ac can be produced via various routes as mentioned above, the most popular method which is currently followed is by separating minute amounts of Ac-225 from its parent ^{229}Th. ^{225}Ac is a member of the decay chain of ^{233}U (Figure 1). Over the years ^{233}U has been produced by several breeder and research reactors. ^{233}U obtained from these reactors was stored as waste. Over the years, decay of ^{233}U has given rise to significant amounts of ^{229}Th from which small amounts of ^{225}Ac can be isolated. The fact that the half-life of ^{233}U is 1,59,200 years and that of ^{232}Th is 7340 years and, that the ^{233}U has only been produced in the past 40-60 years, it is easy to understand how much small amounts of ^{225}Ac are separable from ^{233}U. Also, the separation process needs to be extremely efficient to isolate small quantities of ^{225}Ac from ^{233}U stockpiles. Nevertheless, this is currently the primary method of production of ^{225}Ac.

In this method, the ^{233}U stockpile is dissolved in nitric acid and passed through an ion exchanger. Thorium gets selectively sorbed on the column which is eluted and sent to the isotope production laboratory. At the isotope production laboratories, ^{225}Ac is isolated from ^{229}Th utilizing a series of anion and cation exchangers. A method that has been utilized at ORNL for years involves the use of 6 ion-exchange columns. The process starts with the loading of anion exchanger MP1 followed by washing in which Ac/Ra are coeluted first, while Th gets retained on the column. The traces of Th are removed utilizing another small MP1 column. The ^{225}Ac fraction free from ^{229}Th is then again loaded on anion exchangers to remove traces of Fe (III), Uranium, etc. In the final process, a cation exchanger AG 50 x4 is used to remove the impurities like Ra, Bi, and Pb [10].

Summary

^{225}Ac is undoubtedly a promising radioisotope. In the last few decades, numerous processes have been developed and established to produce ^{225}Ac. However, only a few of these can produce ^{225}Ac in sufficient quantities. Currently, the annual global supply of ^{225}Ac stands at only 63 GBq (1.7 Ci), catering to less than thousand 1000 patients per year. The current world requirement for ^{225}Ac is at least 185 MBq (5 Ci) and increasing every day. Hence, while ^{225}Ac is truly a revolutionizing radioisotope for TAT, the challenges encountered concerning targets for irradiation, radio-nuclidic purity, limited availability of high-energy LINACs, as well as extremely involved chemical processing make ^{225}Ac very less accessible and is currently still the rarest drug on our planet. Nevertheless, efforts are underway world-over to scale up the production processes and obtain ^{225}Ac in adequate amounts for benefit of the mankind.

References

1. Lassmann M, Eberlein U. "Targeted alpha-particle therapy: imaging, dosimetry, and radiation protection". Annals of the ICRP 47/3-4 (2018) 187-195. DOI:10.1177 /0146645318756253

2. Available online: http://www.nucleide.org; accessed on August 17, 2021.

3. McDevitt M R, Ma D, Lai L T, Simon J, Borchardt P, Frank R K, Wu K, Pellegrini V, Curcio M J, Miederer M, Bander N H, Scheinberg D A. "Tumor therapy with targeted atomic nanogenerators". Science. 294/5546 (2001) 1537-40. DOI: 10.1126/science.1064126.

4. Friedlander G, Kennedy J W, Macias E S, Miller J M. In: Nuclear and Radiochemistry, (1981) ISBN: 978-81-265-4080-8.

5. Kratochwil C, Frank B, Frederik L G, Mirjam Weis, Frederik A Verburg, Felix Mottaghy, Klaus Kopka, Christos Apostolidis, Uwe Haberkorn and Alfred Morgenstern. "^{225}Ac-PSMA-617 for PSMA targeting alpha-radiation therapy of patients with metastatic castration-resistant prostate cancer". J. Nucl. Med. 57/12 (2016) 1941-1944. jnumed.116.178673; DOI: 10.2967/jnumed.116.178673.

6. ITU Annual Report 1995-(EUR 16368)-Basic Actinide Research. (1995). "Methods for the production of Ac-225 and Bi-213 for alpha immunotherapy" pp. 55-56.

7. Turner J E, Atoms, Radiation and Radiation Protection, Oak Ridge, TN: WILEY-VCH, (2007) ISBN: 9783527406067.

8. Apostolidis C, Molinet R, McGinley J, Abbas K, Möllenbeck J, Morgenstern A. "Cyclotron production of Ac-225 for targeted alpha therapy". Appl. Radiat. &Isotop. 62/3 (2005) pp-383-387.https://doi.org/10.1016/j.apradiso.2004.06.013.

9. Harvey J T*, "NorthStar Perspectives for Actinium-225 Production at Commercial Scale". Curr. Radiopharma. 11/3 (2018)https://

doi.org/10.2174/1874471011666180515123848.

10. Rose A. Boll, DairinMalkemus, SaedMirzadeh. "Production of actinium-225 for alpha particle mediated radioimmunotherapy". Appl. Radiat. & Isotop. 62/5 (2005) pp-667-679,https://doi.org/10.1016/j.apradiso.2004.12.003.

TECHNOLOGIES FOR
NEW INDIA@75
आज़ादी का अमृत महोत्सव

Compiled, Edited and Published by
Dr. Tarveen Karir
Sr. Manager, Scientific Information Resources & Publications,
Technical Services Division,
Board of Radiation & Isotope Technology, DAE

Printed by
M/S Sundaram Art Printing Press
Wadala, Mumbai